AD-A070 433 TENNESSEE UNIV SPACE INST TULLAHOMA F/G 20/4
SOME AERODYNAMIC PERFORMANCE CALCULATIONS ON MISSILE CONFIGURAT--ETC(U)
MAY 79 J M WU, T H MOULDEN, K SURYANARAYANAN DAAG29-77-G-0108
UNCLASSIFIED ARO-14966.2-A-E NL

| OF |
AD
A070433

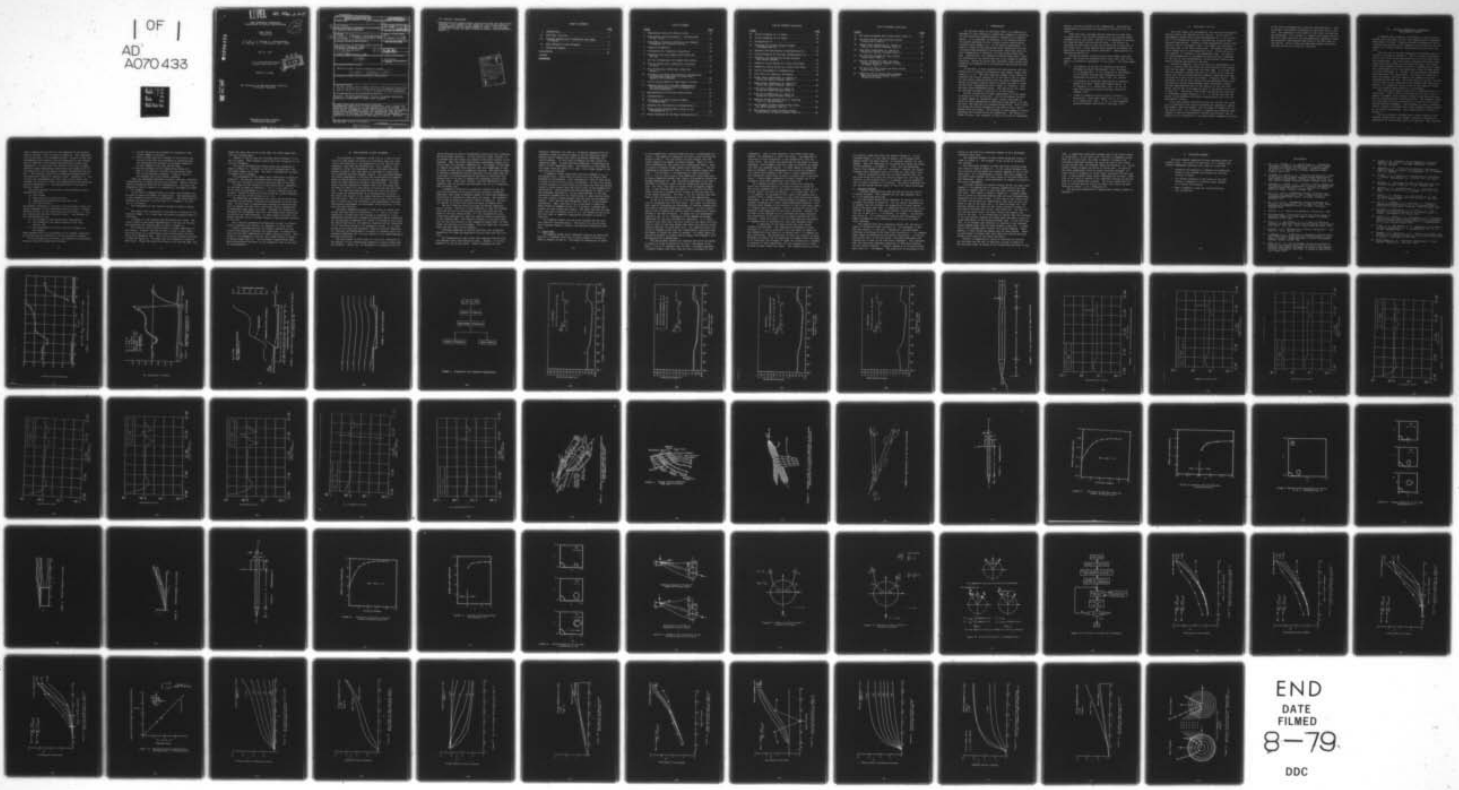

END
DATE
FILMED
8-79
DDC

ARO 14966.2-A-E

SOME AERODYNAMIC PERFORMANCE CALCULATIONS ON MISSILE CONFIGURATIONS

FINAL REPORT
Prepared By

J. M. Wu, T. H. Moulden, K. Suryanarayanan,
N. Uchiyama, R. P. Mikkilineni, and Y. Niwa

May 31, 1979

U. S. Army Research Office
Durham, North Carolina

DAAG29-77-G-0108

The University of Tennessee Space Institute
Tullahoma, Tennessee

Unclassified

SECURITY CLASSIFICATION OF THIS PAGE (When Data Entered)

REPORT DOCUMENTATION PAGE

READ INSTRUCTIONS BEFORE COMPLETING FORM

1. REPORT NUMBER

2. GOVT ACCESSION NO.

3. RECIPIENT'S CATALOG NUMBER

(9)

4. TITLE (and Subtitle)

(6) SOME AERODYNAMIC PERFORMANCE CALCULATIONS ON MISSILE CONFIGURATIONS.

5. TYPE OF REPORT & PERIOD COVERED

FINAL REPORT, 15 Jan 1977- 30 Nov 1978

6. PERFORMING ORG. REPORT NUMBER

7. AUTHOR(s)

(10) J. M. Wu, T. H. Moulden, K. Suryanarayanan, N. Uchiyama, R. P. Mikkilineni, and Y. Niwa

8. CONTRACT OR GRANT NUMBER(s)

(15) DAAG29-77-G-0108

9. PERFORMING ORGANIZATION NAME AND ADDRESS

The University of Tennessee Space Institute
Tullahoma, Tennessee 37388

10. PROGRAM ELEMENT, PROJECT, TASK AREA & WORK UNIT NUMBERS

11. CONTROLLING OFFICE NAME AND ADDRESS

(11) 31

U. S. Army Research Office
P. O. Box 12211
Research Triangle Park, NC 27709

12. REPORT DATE

May 1979

13. NUMBER OF PAGES

14. MONITORING AGENCY NAME & ADDRESS (if different from Controlling Office)

(12) 84p.

15. SECURITY CLASS. (of this report)

Unclassified

15a. DECLASSIFICATION/DOWNGRADING SCHEDULE

16. DISTRIBUTION STATEMENT (of this Report)

Approved for public release; distribution unlimited.

(18) ARO (19) 14966.2-A-E

17. DISTRIBUTION STATEMENT (of the abstract entered in Block 20, if different from Report)

18. SUPPLEMENTARY NOTES

The view, opinions, and/or findings contained in this report are those of the author(s) and should not be construed as an official Department of the Army position, policy, or decision, unless so designated by other documentation.

19. KEY WORDS (Continue on reverse side if necessary and identify by block number)

Missiles, fin-body combinations, cut-out, jet-plume interaction, moderate to high angle of attack, nose vortices.

20. ABSTRACT (Continue on reverse side if necessary and identify by block number)

Axisymmetric bodies with a clean configuration have a rather flat pressure distribution on the cylindrical portion of the body. In this report, axisymmetric bodies with surface cut outs are modelled using an inviscid flow approach with experimental flow results. Literature is available on numerical schemes for aerodynamic calculations on fins at moderately high angles of attack. Fin-body

over

DD FORM 1 JAN 73 1473 EDITION OF 1 NOV 65 IS OBSOLETE

Unclassified

SECURITY CLASSIFICATION OF THIS PAGE (When Data Entered)

387070

LB

20. Abstract (Continued)

combinations are studied using a nose vortex model and some results reported. Also studied is the asymmetric nose vortex problem on an axisymmetric body at higher angles of attack. This has been studied for conical and ogive forebodies using a modified Wardlow's method.

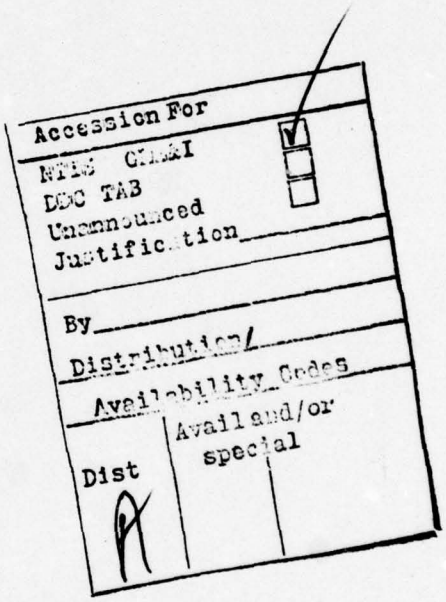

TABLE OF CONTENTS

		PAGE
I.	INTRODUCTION	1
II.	FLOW PAST A CUT OUT	3
III.	FIN-BODY COMBINATION AT MODERATELY HIGH ANGLE OF ATTACK	5
IV.	NOSE VORTICES AT HIGH INCIDENCE	9
V.	CONCLUDING REMARKS	17
BIBLIOGRAPHY		18
FIGURES		
~~APPENDICES~~		

LIST OF FIGURES

FIGURE		PAGE
1.	Experimental Result On Shallow Cavity	20
2.	Experimental and Calculated C_p - Distributions at $M_\infty = 0.84$	21
3.	Experimental Pressure Coefficient and Computed Streamline For A Shallow Cut Out	22
4.	Computed Streamlines	23
5.	Formulation For Streamline Computation	24
6.	Streamline Plot and Computational Model For Cut Out	25
7.	Cut Out Configuration For Sample Calculation	29
8.	Plot Of Section Lift Coefficient Along Body Surface	30
9.	Plot Of Pressure Coefficient Along Body Surface	33
10.	Schematic Flow Field Around Missile Configuration At Moderately High Angle Of Attack With Emphasis On Fin Effects	39
11.	Vortex Lattice Method At High Angle of Attack	40
12.	Schematic Model Of A Fin-Body Combination In The Present Analysis With An Exaggerated Fin-Body Combination	41
13.	Representation Of The Nose Vortex System	42
14.	Configuration I	43
15.	Variation of C_N With Iteration Number (Configuration)	44
16.	Spanwise Lift Distribution (Configuration I)	45
17.	Vortex System Including Nose Vortex At x=1 (Configuration I)	46
18.	Vortex Formation On The Wing (Configuration I)	47

LIST OF FIGURES (Continued)

FIGURE		PAGE
19.	Vortex Filaments In x-y Plane	48
20.	Vortex Filaments In x-z Plane	49
21.	Configuration II	50
22.	Variation Of C_N With Iteration Number (Configuration II)	51
23.	Spanwise Load Distribution (Configuration II)	52
24.	Vortex Formation On The Wing (Configuration II)	53
25.	Schematic and Coordinates Of Two Possible Nose Vortex Systems	54
26.	Symmetric Vortex System In a Cross Flow Plane	55
27.	Asymmetric Vortex System In a Cross Flow Plane	56
28.	Initial Development of Asymmetricity	57
29.	Flow Chart for Numerical Procedures	58
30.	Normal Force Coefficient vs. Angles of Attack For Ogive Forebody (Case 1)	59
31.	Normal Force Coefficient vs. Angles of Attack For Ogive Forebody (Case 2)	60
32.	Side Force Coefficient vs. Angles of Attack For Ogive Forebody (Case 1)	61
33.	Side Force Coefficient vs. Angles of Attack For Ogive Forebody (Case 2)	62
34.	Absolute Vortex Strength Ratio At Starting Point vs. Distance Ratio	63
35.	The Strength Of Outer Vortex Along x-Axis For Ogive Forebody (Case 2)	64
36.	The Strength Of Inner and Outer Vortex Along x-Axis For Ogive Forebody (Case 2)	65

LIST OF FIGURES (Continued)

FIGURE		PAGE
37.	The Vortex Strength Ratio Along x-Axis (Case 1).....	66
38.	The Trace Of The Inner and Outer Vortex Along x-Axis (Case 2).....	67
39.	Normal Force Coefficient vs. Angles of Attack For Conical Forebody (Case 2).....	68
40.	Side Force Coefficient vs. Angles Of Attack For Conical Forebody (Case 2).....	69
41.	The Absolute Strength Of Outer Vortex Along x-Axis (Case 2).....	70
42.	Absolute Strength Of Inner and Outer Vortex At 40 and 55 Degrees In Angle Of Attack (Case 2).....	71
43.	The Trace Of Inner Vortex and Outer Vortex Along x-Axis (Case 2).....	72
44.	Comparison Of The Vortex Traces Between Ogive and Conical Forebody (Case 2) (Viewed From Front).....	73

I. INTRODUCTION

Our previous years of continuous effort (as summarized in Reference 1) have resulted in significant progress in analyzing the flow field over powered missiles, especially at transonic speeds. It is important, in addition to our previous efforts, to estimate influence by fins, surface cutouts and different incidence angle ranges, etc., to the missile performance. In order to obtain an inviscid/viscous flow interaction solution, a complete understanding of the potential flow field about missile configuration is required. We have worked toward this goal. Nevertheless, the originally planned three years' effort was terminated at the second year due to the change in funding situation. During the period work performed, three papers were prepared and presented in an international meeting and national meetings.

In the past, we have analyzed flow over missiles with cruciform fins in subsonic and supersonic Mach Number ranges (References 1, 2, 3). The above includes studies on the effect of viscosity and viscous interaction of the flow on the jet plume. All the results reported hereto were for clean configurations. During the present contract period an effort was made to study the flow over configurations with "steps" or "cutouts". This was done using slenderbody theory. The results of this study are reported in detail in Section II of this report.

We have studied the fin-body combinations at lower angles of attack up to 10° in the past. Due to the growing interest in higher angles of incidence flight, efforts were made to study fin body combinations at moderately high angles of attack. For fins, the wake has to be modelled effectively. This is done by letting the vortex filaments in the wake to float, and to decide their own course. The forebody at these angles of attack generates two vortices which are symmetrical. The effects of these vortices, (the strengths of which are given by slenderbody

theory), are also included in the computations. The detailed investigations and results are reported in Section III of this report.

There has been a growing interest exhibited in high angle of attack flows. The vortices generated by the forebody become unsymmetrical at this point, and due to the shedding of vortices, the large and small vortices switch sides. This results in switching of directions of side forces which are of the order of the normal force. These effects were studied by extending our method for the ogive and conical forebodies. These results are reported in Section IV.

During the present contract period three papers were published. The titles are presented below, and a full copy of the papers is included in appendices to this report. The three papers are:

1. "An Analysis of Various Fin Geometries and Their Influence on Rocket Performance", by N. Uchiyama, T. H. Moulden and J. M. Wu, presented at Proceedings of the Twelfth International Symposium on Space Technology and Science, Tokyo, 1977, pp. 109-120.

2. "An Analysis of Wing-Body Combinations at Moderate Angles of Attack", (AIAA Paper Number 78-62), by N. Uchiyama, R. P. Mikkilineni, and J. M. Wu, at AIAA 16th Aerospace Sciences Meeting, Huntsville, Alabama, 1978.

3. "Study of Asymmetric Nose Vortices of Bodies of Revolution", (AIAA Paper Number 79-27), by Y. Niwa, R. P. Mikkilineni, and J. M. Wu, at 17th Aerospace Sciences Meeting, New Orleans, Louisiana, 1979.

II. FLOW PAST A CUT OUT

Flow over bodies with axisymmetric cut outs was investigated, and the results are reported in this section. In the case of axisymmetric bodies with a clean configuration (i.e., no cut outs etc.,) the cylindrical portion of the body has an almost flat pressure distribution. Looking at some experimental results (References 4 and 5) in Figures 1 and 2, we clearly see the effect the cavity has on the nearly sonic flow. The results reported in those figures are for two-dimensional flows. If the cut out is very shallow, it is nearly a two-dimensional flow. As results for three-dimensional or axisymmetric flows were not accessible at the time of this investigation, two-dimensional results were used in studying the nature of the flow.

Looking at Figures 1 and 2 (and some more experimental results), it can be seen that there are re-circulatory flow regions near the two edges, longer near the front edge. It is hence possible to consider a stream line that is closest to the body and passes over the re-circulatory flow regions (treating those regions more as a part of the solid body). (Figures 3 and 4). This technique, it can be seen, would avoid the detailed viscous flow calculations and the shock-boundary layer interaction studies. The main approximation made in the analysis is that the flow enters the cut out at an angle of about 7° and leaves the cut out at about 45°. The results from these calculations are reported in subsequent figures (Figures 5 - 9). It can be seen that the nature of the pressure distribution agrees pretty well with the experimental results.

Also, the pressure distribution over the cavities was found to be a function of the three non-dimensional parameters, namely, Mach Number, Reynold's Number, and the height to length ratio of the cavity (h/L). It is possible to compute the streamline shape (Figure 5) from the experimental pressure distribution, and an equation can be formulated to the approximated streamline in terms

of the three non-dimensional parameters mentioned above. This technique is essentially computing the equivalent body in the flow. The advantage of this method is that once the equations are formulated, it is possible to compute the pressure distribution at other values of the non-dimensional parameters using the equivalent body approach mentioned in the first part of the section. Such a study was undertaken during the present contract period, but it was not completed.

III. FIN-BODY COMBINATION AT MODERATELY HIGH ANGLE OF ATTACK

A computational technique is developed to study the aerodynamic flow over wing (or fin) body combinations at moderately high angles of attack. Numerical results including the static stability derivatives and the damping in pitch and roll are presented for a typical missile configuration with fins and canards.

The flow over a fin-body combination at moderate angles of attack is sketched in Figure 10. One of the main characteristics of this flow is the separated flow at the fin tips and/or the leading edge. The vortex sheet separated from these sharp edges rolls into strong vortices above the wing. The strong cross flow produced by these vortices is responsible for larger lift coefficients of the low aspect-ratio wings at high angles of attack (Reference 6). Further, this interaction introduces non-linearities into the problem. For angles of attack up to about 25 degrees, the body supports two symmetric vortices originating from the nose. For these angles of attack, the flow over the body is not separated on the leeward side, and consequently, the asymmetric vortex system of high angle of attack flow over slender bodies need not be considered.

The bound vortex sheet of the fins is represented by a vortex lattice. This is done by dividing the fin into a finite number of elements each carrying a bound vortex along the span and two trailing vortices along the chord. The separated sheets from the edges and tips are modelled by a series of non-intersecting vertical filaments. Each filament in turn is represented by a series of straight line vortex segments joined together at the points called nodes. This representation is shown in Figure 11.

The body surface is divided into a finite number of rectangular elements with each element carrying a concentrated singularity of source-sink type at its centroid. This represen-

tation assumes that the flow is not separated on the leeward side of the body. This is shown in Figure 12. The representation of the nose is not straight forward. One has to take into consideration the potential vortices generated by the lifting nose in addition to the surface distribution of source type singularity. In this work, the surface of the nose is represented by using concentrated source-sink type singularities at the centroids of the rectangular elements representing the surface. The potential vortices are represented based either on the theoretical results or empirical data. (Reference 7). The vortices are represented by a horse shoe vortex system, the strength and location of which are predetermined from empirical relations (Reference 7). The representation of the nose is shown in Figure 13.

The total velocity on the body is the resultant of the contributions from:

a) free stream
b) body rotation in pitch and roll
c) singularity distribution on the body; and
d) the free vortices

The boundary condition on the body to be satisfied is that the normal component of this resultant velocity be zero. Further, the free vortices in the vortex wake are force free i.e., they are aligned with the local velocity vector. The unknowns in this representation are:

a) the strength of the concentrated singularities
b) the strength of the bound vortices on the wing surface, and
c) the orientation of the free vertical filaments in the stream.

These unknowns are to be determined by the boundary conditions on the body and the condition on the free vertical elements.

As this problem is non-linear, the unknowns are determined using an iterative scheme which includes:

a) Initial direction and strength are assigned to each vortex element in the wake.

b) With the wake fixed the strength of the vortices and sources on the body are determined by requiring that the resulting flow satisfies the boundary condition on each element of the body and the wing.

c) With the strength of the singularities fixed the wake is re-oriented to satisfy the force-free condition on the vertical filaments. Steps (b) and (c) are repeated until the iterates converge.

Using the technique discussed in earlier sections, different configurations of typical missiles are analyzed. Results are presented in graphical form for two configurations. The first configuration shown in Figure 14 is analyzed for the angle of attack α = 19.4 degrees.

As the flow is symmetric about x-z plane, this property can be used to reduce the number of computations. The representation is only needed for half of the configuration. The discretization involves the division of the fin into 5 x 5 elements, the body into 6 x 12 panels.

The convergence of the iteration scheme is shown in Figure 15.

The normal force coefficient is plotted as a function of the iteration number. It is seen that the process converged within 8 iterations.

In Figure 16, the spanwise load distribution is shown. The vortex system in the plane perpendicular to the axis of the body and containing the trailing edge is shown in Figure 17.

The rolled up vortex from the wing is clearly identified in this figure. Further, the nose vortex is shown in this figure. The nose vortex is a concentrated vortex located above the body about three diameters away. The roll-up of the separated vortices is shown in Figure 18. In Figure 18a, the formation is shown at half chord. Figure 18b shows the vortex at the trailing edge, and

Figure 18c shows the vortex in the wake, one chord length away from the trailing edge.

Figures 19 and 20 show the trailing vortex filaments in x-y and x-z planes. These figures clearly show the rolling up of the vortical filaments.

The second configuration studied using this technique is shown in Figure 21. Compared to the first configuration, this has higher aspect ratio wing. The flow is analyzed for an angle of attack of 19.4 degrees.

The convergence of the normal force coefficient is shown in Figure 22. The process converged within 8 iterations. Figure 21 shows the variation of the load along the span of the wing.

In Figure 24 the formation of the vortex due to separation on the wing is shown at stations $x = 0.5$, $x = 1.0$, and $x = 2$. In the wake corresponding to $x = 2$, a clearly formed vortex can be seen. Figure 16 shows the vortex system in a plane perpendicular to the axis of the missile at $x = 1.0$.

The modelling and computation of a flow over fin-body combinations for any angle of attack and orientation is not an easy task. In this work, a computational technique is described and used to compute the flow over a practical missile configuration at moderately high angles of attack. Although the results are presented for rectangular fins only, the scheme could effectively be used for any other planform. At these angles of attack, the linear theories are not suitable because of the nonlinear behavior of the flow.

For a detailed mathematical formulation as well as computational procedures and results, see Appendix 2 of this report.

Further knowledge and work are needed, especially on the viscous flow behavior including flow separation, to effectively treat the fin-body combinations at higher angles of attack. This is due to the asymmetric flow over the slender bodies at angles of attack larger than 25°. Any reasonable computational model should incorporate the aspect of the asymmetric flow in the overall representation.

IV. NOSE VORTICES AT HIGH INCIDENCE

The existence of asymmetric vortex flow on a body of revolution at high angles of attack or at incidence with zero side slip to any plane due to the symmetricity of the body has been observed a long time ago (Reference 8). Until recently, this asymmetric vortex flow phenomenon was not paid much attention because flying at very high angle of incidence is rarely done. This situation has been changed, however. The increasing demand for better performance of missiles has necessitated new improvements in characteristics of missiles at high angles of attack, which can occur during an extremely sharp maneuver. The asymmetric vortices generate an induced side force and yawing moment when the body is at high angles of attack and has zero side slip. The side force and yawing moment may force the missile into either an uncontrollable or an unpredictable situation. The worse case results in the sudden switching of direction of the side force. Much of the research work on the study of asymmetric vortex flow, both theoretical and experimental, has been done because improvement of aerodynamic characteristics in this area has been required.

Excellent background reviews on high angle of attack technology have been given in References 9 - 11. One of the basic approaches of using cross flow analogy by appealing to a two-dimensional analysis was originally proposed by Bryson (Reference 12) and Angelucci (Reference 13), which is followed by this study. The method used here is the Wardlaw's modified version (Reference 14) of cross-flow analogy to an asymmetric system. It is interesting to note here that Sarpkaya's impulsive analogy (Reference 15), Marshall and Deffenbaugh's inclusion of boundary-layer contribution (Reference 16), are also helpful to our understanding of lee-side vortex flow.

The main object of this study is a first-cut estimation on the behavior of two concentrated asymmetric vortices formed near the forebody. Fidler, et. al (Reference 17) indicated that the

vortex flow may not have a concentrated vortex core but a diffused and distributed vorticity. In this first-cut study, however, it is assumed that the vortex core exists in the front portion of the forebody. Many flow field visualization experiments support this notion (See, for instance, Reference 18). An attempt is then made to compute the normal force and the side force magnitudes as well as traces of this pair of asymmetric vortices. The previous paper of Uchiyama, Mikkilineni and Wu (Reference 19) has shown that the first pair of vortices generated by any body of revolution with pointed nose is the key to leading the subsequent vortices from the main body. Their work, however, has been addressed to the symmetric pair of vortices and applicable only up to a moderately high incidence case.

A symmetric vortex flow is generally observed on the leeward side of bodies of revolution in the subsonic to moderate supersonic flow range at moderate angles of attack and asymmetric vortex flow is observed at high angles of attack. The schematic flow fields on these two cases are shown in Figure 25. The vortex systems in a cross flow plane are shown in Figures 26-27.

The two conditions used in solving the motion completely are as follows: The first of the conditions is that the feeding sheet and the roll-up concentrated vortex must have zero net force on the free vortex system. So, the concentrated vortex itself must experience an equal but opposite force as generated by the feeding sheet. The second is similar to the Kutta condition in that the location of the stagnation points where the flow leaves the body has to be assigned. They are taken here as points where the wall sheer stress vanishes.

Governing equations as derived previously are integrated numerically by using the Runge-Kutta routine with step size control.

The integration of wake vortex flow requires starting from the boundary layer flow separation point. However, it is very difficult to set up this point. Bryson (Reference 12) and

Angelucci (Reference 13) used θ_0 = 40 degrees measured from the horizontal plane as shown in Figure 3 for the separation angle. Wardlaw used 42 degrees and Clark and Peoples (Reference 20) used 65 degrees. In this study 40 degrees has been chosen for separation angle. A study has been conducted to investigate the effect of this separation angle. The influence of this angle on the normal force was found to be small, but a large change in the side force was observed.

A symmetric vortex system which has the strength of λ_{st} is calculated first. After that an *asymmetricity* by using a free parameter is instroduced. This asymmetricity, used in this study, is given by one of the following two methods. In the first method, a vortex position is artificially moved toward the body and another vortex is moved outward from the body in half of the asymmetricity, respectively. This procedure has been designated as "Case 1" in the subsequent calculation. In the second method, it has been arbitrarily assumed that one vortex keeps its same position while the other vortex is moved outward from the body in an asymmetric pattern. This case has been designated "Case 2" in the present calculation. Case 1 and Case 2 are illustrated in Figure 28. Three values of asymmetricities of 0.5 percent, 1 percent and 2 percent of local radius are studied. The ogive nose and the cone nose, both with a fineness ratio of 3.5, are chosen in this study. The flow chart of numerical computation procedure is given in Figure 29.

The computer results for the ogive forebody and the cone-nose cases are discussed below. The results for the two cases are in general similar; however, some distinct differences also exist.

1. Ogive Nose

The computed normal force component acting on an ogive forebody of 3.5 fineness ratio and at various angles of attack are shown in Figures 30 and 31. The Figure 30 computation is based

on the asymmetricity starting condition Case 1 as described previously. The Figure 31 computation is based on the starting condition of Case 2. The two results are very similar over the entire range of the angles of attack studied. There is a very minute difference in the normal force coefficient values. Case 2 predicts a slightly larger normal force than Case 1. The corresponding circulation for Case 2 is also slightly larger than Case 1. For the Case 1, the magnitude of total circulation ($|\lambda_1| + |\lambda_2|$) is very close to the symmetrical vortex flow case by using a modified slender body theory as proposed by Fidler and Bateman (Reference 21). The circulation generated by the Case 2 procedure is slightly larger than the symmetrical vortex flow case. For Case 1 and angle of attack below 30 degrees computation, it was observed that the smaller, or closer-to-the-body inner vortex has a tendency first to move in and then move out in the radial direction. For Case 2, the two vortices have been shown to move out monotonically in all of the computations.

As far as in the reality, it is not known how the asymmetricity is introduced into the flow field. The values of free parameter used in indicating the percentage of starting asymmetricity are shown in the above-mentioned two figures. At this stage we have no way of knowing the correct value of asymmetricity corresponding to the real situation. In Figure 30, two experimental results by Coe, et al. (Reference 18) and Chapman and Keener (Reference 22) are also included for comparison. It is interesting to note that these two sets of data do not agree with each other in spite of the data having been taken over similar configurations and with the same model size. Our computed results are closer to Chapman's data than Coe's measurement, especially when the angles of attack are below 45 degrees. At larger angles of attack the present calculated results depart from Chapman's data and approach Coe's measurement.

The relationship between the computed side force and angles of attack is shown in Figure 32 for Case 1 and Figure 33 for Case 2. How it is observed that the Case 1 procedure generates a slightly higher side force than the Case 2 procedure in this

computation. This is just opposite to the normal force case. However, the difference is still very minute. The magnitude of side force is more susceptible to the asymmetricity than the normal force. The curves are spread more as the angle of attack increases. Both Chapman's and Coe's data are plotted for comparison with the computed results. At lower angles of attack (say below 45 degrees), Coe's measurement lies in the low asymmetricity curves while Chapman's data shows a higher asymmetricity. Our computation showed that in order to achieve such a high side force, a twice-larger asymmetric vortices strength has to be assumed to start the computation (see Figure 34).

The computed results on the outer vortex flow along the x-axis for different angles of attack are shown in Figure 35. The initial asymmetricity in the radial distance is given as two percent (Case 2) in this calculation. It is found that, up to α = 35 degrees, the strength of this vortex flow remains near a constant (with a slight increase) as the vortex flow moves toward downstream. As the angle of attack exceeds 35 degrees, the vortex strength increases as it moves toward downstream direction. This indicates more feeding of the vorticity to the vortex sheet occurs at a higher angle of incidence. This is because the cross-flow component gains magnitude as the U-sinα increases. However, the increase in the strength is in a nonlinear way which indicates the contribution of the dr/dx term is highly coupled with the α influence. From this study, it is also realized that the growth in asymmetricity is nonlinear for very high incidence cases.

A comparison of the inner versus the outer vortex strength has been made. The computed non-dimensional vortex strengths of λ_1 and λ_2 along the x-axis are shown in Figure 36. The asymmetricity was taken as two percent and α = 55 degrees in this calculation. The growth rate of these two vortices is quite different initially, but at downstream it becomes nearly the same. It is found that the strength of these two vortices has a tendency to equalize in their magnitudes, but the asymmetricity in their distance becomes larger and larger. The strength ratios of these

two vortices along the x-axis are shown in Figure 37. As the incidence angle α is less than 35 degrees, the strength ratio remains nearly the same; however, it increases rapidly for $\alpha \gtrsim 40$ degrees. Note the difference in the growth rate along the x-axis for the different α in Figure 27. Also, note the decreasing trend of the strength ratio as α increases. Finally, the vortex strength ratio approaches unity as a limit for very high α case.

Typical calculated traces for the inner and the outer vortex cores along the x-axis are given in Figure 38. For this computation, it was assumed that α = 45 degrees, and the asymmetricity of radial distance is 0.5 percent. The result indicated that two vortices become farther apart as they flow toward downstream.

2. Conical Forebody

A similar computation has been carried out for the case of a conical forebody. This forebody has the same fineness ratio of 3.5 as mentioned previously.

The calculated normal force components at various angles of incidence are shown in Figure 39. For the conical forebody case, it appears that the influence of asymmetricity is much smaller than in the ogive nose case. A comparison with Coe's data is also included in Figure 39. The theory predicts rather well against this set of data up to α = 45 degrees. At higher α, the discrepancy shows up. It is difficult to explain this discrepancy at higher incidence by only considering the variation in normal force component.

The computed side force components against the variation in angles of attack are shown in Figure 40. The agreement of data with the theory is rather poor. Especially, the measurement indicated a switching in the side force direction at α = 40 degrees, which cannot be predicted by the present calculation. In the previous ogive case, it has been shown a reasonable agreement with limited sets of data on the side force components. This indicates that the side force component prediction is much more difficult for the conical forebody. A drastic change in the vortex pattern must occur at α = 40 degrees. The prediction of switching of dir-

ection in the side force component remains to be a formidable problem at this time.

The computed strength of outer vortex along the x-axis is shown in Figure 41. The strength of the vortex is increased very quickly.

The calculated strength of inner and outer vortices along the x-axis is shown in Figure 42. In the conical forebody case, both vortices are developed very quickly compared to that of the ogive case. It is interesting to observe that the strength of the inner vortex exceeds the outer vortex as the flow moves toware downstream. Again, a good experiment is needed to confirm or deny such a phenomenon.

A similar condition as shown in Figure 38 for the ogive case (namely α = 45 degrees and 0.5 percent asymmetricity) has been applied to compute traces of outer and inner vortices for the cone case. This result is shown in Figure 43. A marked difference in traces is observed between these two nose configurations, especially in the outer vortex. In the case of the conical nose, the outer vortex moves out significantly away from the body compared to that of the ogive case -- as shown in Figure 38. The distance between the inner and the outer vortices is larger in the conical forebody case as well (see Figure 43). For both the cone and the ogive cases, the inner vortex core remains very close to the body. It is interesting to observe that the strengths of the two vortices (Figure 42) remain about the same in spite of large differences in the distance between them. In the real flow case, it is probably very difficult to maintain a very extended vortex feeding sheet from the body surface to the core. A breakdown of this feeding sheet results in a vortex shedding. Consequently, a third vortex may appear near the body surface. There is good reason to suspect that this third and close-to-the-body vortex is the cause of side force switching.

Finally, a comparison of traces or positions of vortices for the ogive and the cone is made and is given in Figure 44. The positions shown in Figure 44 are viewed from the front of the

body. A significant difference between each of the vortex traces is illustrated. In the ogive case, the trace is somewhat curved, while in the cone case, the trace is nearly a straight line. A noticeable difference between the ogive and cone is also clear. It may conclude that the forebody radius distribution, i.e., dr/dx, affects rather strongly the motion of vortex flow. In spite of the small asymmetrical value in radius initially assigned, the final result in asymmetry is quite large, especially for the cone case. A check against Föppl theory (Reference 23) is made. Föppl line is the locus of centers of two symmetric vortices on the lee-side of a two-dimensional cylinder. Our result showed that the path of vortices does not follow the Föppl line, which was also observed by Fidler, et al. (Reference 17).

The detailed formulation of computational scheme is given in Appendix 2.

V. CONCLUDING REMARKS

The above remarks summarize the work performed under the present study. As a result of this work, it is evident that several fundamental questions still need to be resolved.

1. Potential flow analysis is adequate for predicting forces if the strength and location of the free-vortices is known.
2. The initial formation of the vortex on the body (either a forebody or a lifting planar surface) is a viscous flow problem.
3. Work is needed to study this viscous/inviscid flow interaction.

BIBLIOGRAPHY

1. Wu, J. M., Moulden, T. H., and Uchiyama, N., "Aerodynamic Performance of Missile Configurations at Transonic Speeds Including the Effects of a Jet Plume", Technical Report RD-76-23, U. S. Army Missile Command, Redstone Arsenal, Alabama, March 1976.

2. Uchiyama, N., and Wu, J. M., "Inviscid Flow Analysis on Body of Revolution with Slender Cruciform Canted Delta Fins at Small Angle of Incidences", Technical Report RD-75-32, U. S. Army Missile Command, Redstone Arsenal, Alabama, March 1975.

3. Uchiyama, N., and Wu, J. M., "A Study of Various Slender and Non-Slender Fin-Body Combinations of Missile Configurations", Technical Report RD-CR-76-5, U. S. Army Missile Command, Redstone Arsenal, Alabama, November 1976.

4. Wu, J. M., et al., "Fundamental Studies of Subsonic and Transonic Flow Separation", Part I, AEDC-TR-75-95, Arnold Engineering Development Center, Tullahoma, Tennessee, September 1975.

5. Wu, J. M., et al., "Fundamental Studies of Subsonic and Transonic Flow Separation", Part II AEDC-TR-77-103, Arnold Engineering Development Center, Tullahoma, Tennessee, December 1977.

6. Nielsen, J. N., "Missile Aerodynamics", McGraw-Hill, 1960.

7. Belotserkovskii, "Calculation of the Flow Around Wings of Arbitrary Planform in a Wide Range of Angles of Attack", NASA-TT-F 12,991, 1969.

8. Allen, H. J., and Perkins, E. W., "A Study of Effects of Viscosity on Flow Over Slender Inclined Bodies of Revolution," NACA Report 1048, 1951. Also, Allen's NACA RM A9126, 1949.

9. Nielsen, J. N., "Nonlinearity in Missile Aerodynamics," AIAA Paper No. 78-20, January 1978.

10. Jorgensen, L. H., "Prediction of Aerodynamic Characteristics for Slender Bodies Alone and With Lifting Surfaces to High Angles of Attack," AGARD High Angle of Attack Aerodynamics Meeting, Norway, October 1978.

11. Baker, W. B., Jr., "An Aerodynamic Coefficient Prediction Technique for Slender Bodies With Low Aspect Ratio Fins at Transonic Mach Numbers and Angles of Attack to 180 Degrees," Doctoral Dissertation, University of Tennessee Space Institute, August 1976.

12. Bryson, A. E. "Symmetric Vortex Separation on Circular Cylinders and Cones," J. of Appl. Mechanics, December 1959, pp. 643-648.

13. Angelucci, S. B. "A Multivortex Method for Axisymmetric Bodies at Angle of Attack," J. of Aircraft, Vol. 8, December 1971, pp. 959-966.

14. Wardlaw, A. B. "Prediction of Yawing Force at High Angle of Attack," AIAA Journal, pp. 1142-1144, Vol. 12, August 1974.

15. Sarpkaya, T. "An Analytical Study of Separated Flow About Circular Cylinder," ASME, pp. 511-520, December 1968.

16. Marshall, F. J., and Deffenbaugh, F. D. "Separated Flow Over a Body of Revolution," J. Aircraft, No. 2, Vol. 12, 1975.

17. Fidler, J. E., Nielsen, J. N., and Schwind, R. G. "An Investigation of Slender-Body Wake Vortices," AIAA Paper No. 77-7, January 1977.

18. Coe, P. L., Chambers, J. R., and Letko, W. "Asymmetric Lateral-Directional Characteristics of Pointed Bodies of Revolution at High Angles of Attack," NASA TN D-2095, 1972.

19. Uchiyama, N., Mikkilineni, R. P., and Wu, J. M. "The Analysis of Wing-Body Combinations at Moderate Angles of Attack," AIAA Paper 78-62, January 1978.

20. Clark, W. H., Peoples, J. R., and Briggs, M. M. "Occurrence and Inhibition of Large Yawing Moments During High-Incidence Flight of Slender Missile Configuration," J. of Spacecraft, Vol. 10, pp. 510-519, August 1973.

21. Fidler, J. E., and Bateman, M. C. "Asymmetric Vortex Effects on Missile Configurations," J. of Spacecraft, Vol. 12, pp. 675-681, November 1975.

22. Chapman, G. T., and Keener, E. R. "Onset of Aerodynamic Side Forces at Zero Sideslip on Symmetric Forebodies at High Angles of Attack," AIAA Paper 74-770, 1974.

23. Milne-Thomson, L. M. "Theoretical Hydrodynamics," Third Edition, MacMillan Co., New York, 1955.

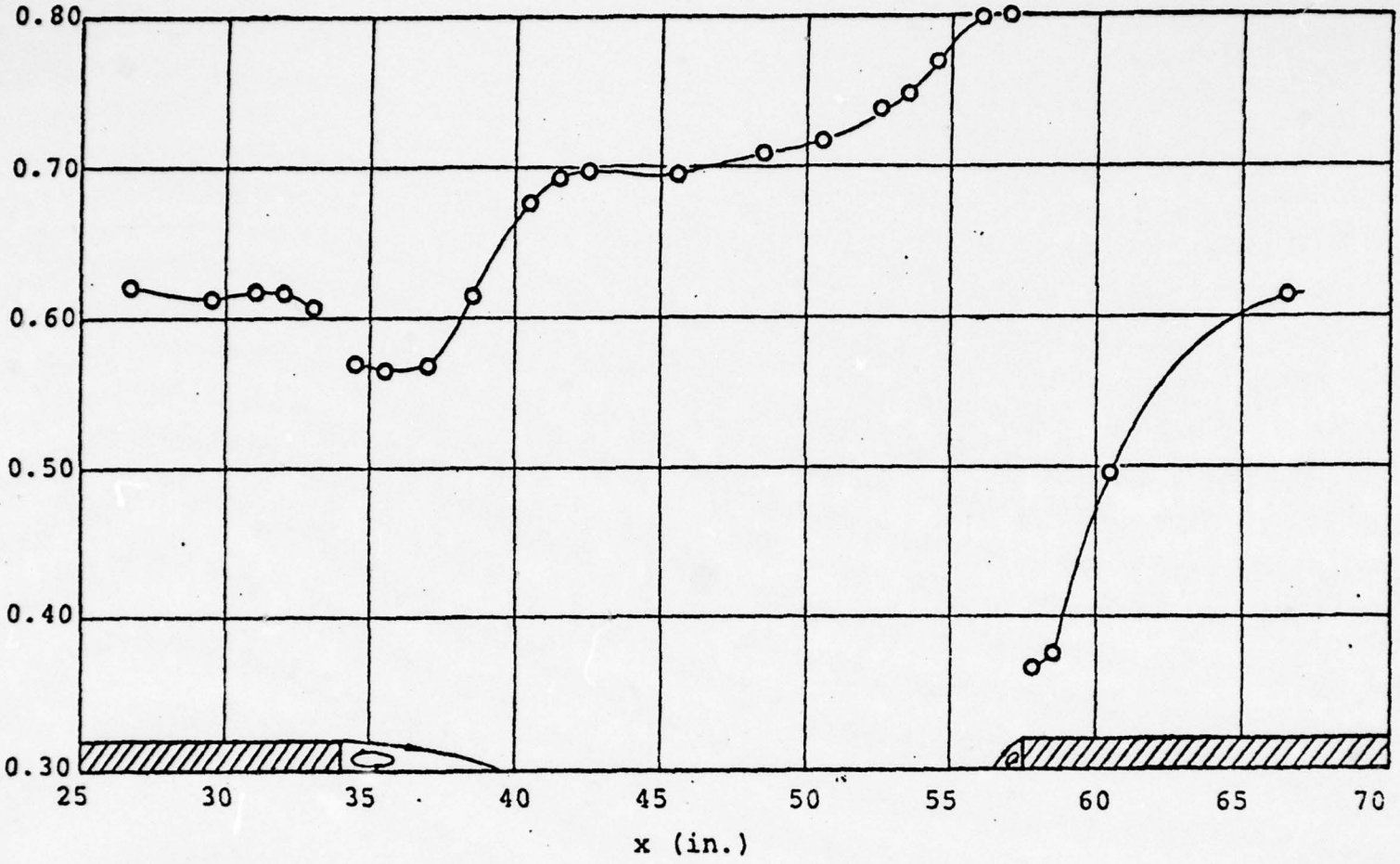

$M_\infty = 0.85$, $Re_{L_R} = 37.0 \times 10^6$, h = 1 inch

FIGURE 1. Experimental Result On Shallow Cavity (Ref. 5)

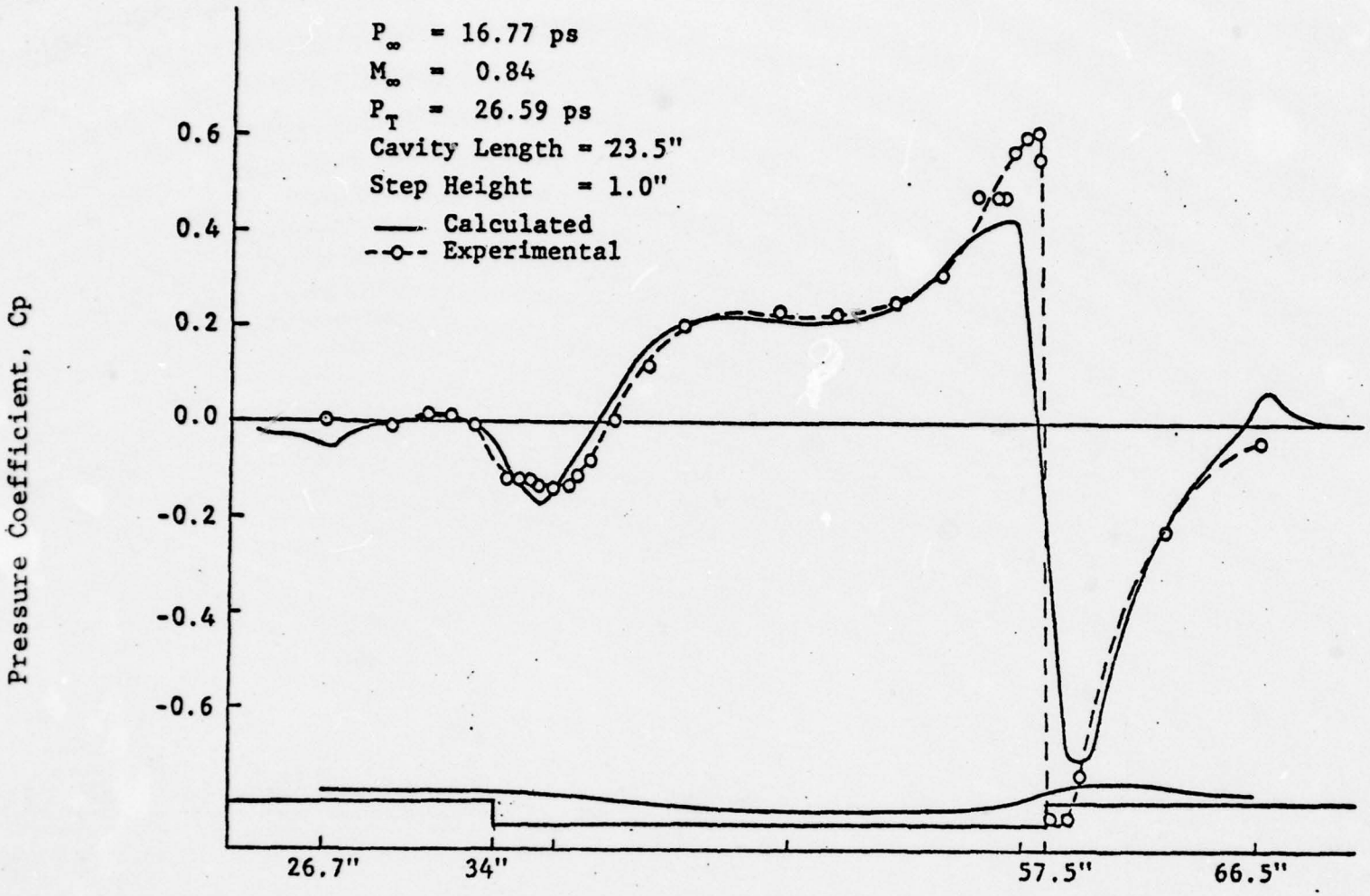

Figure 2. Experimental and calculated C_p - distributions at M_∞ = 0.84. (Reference 5)

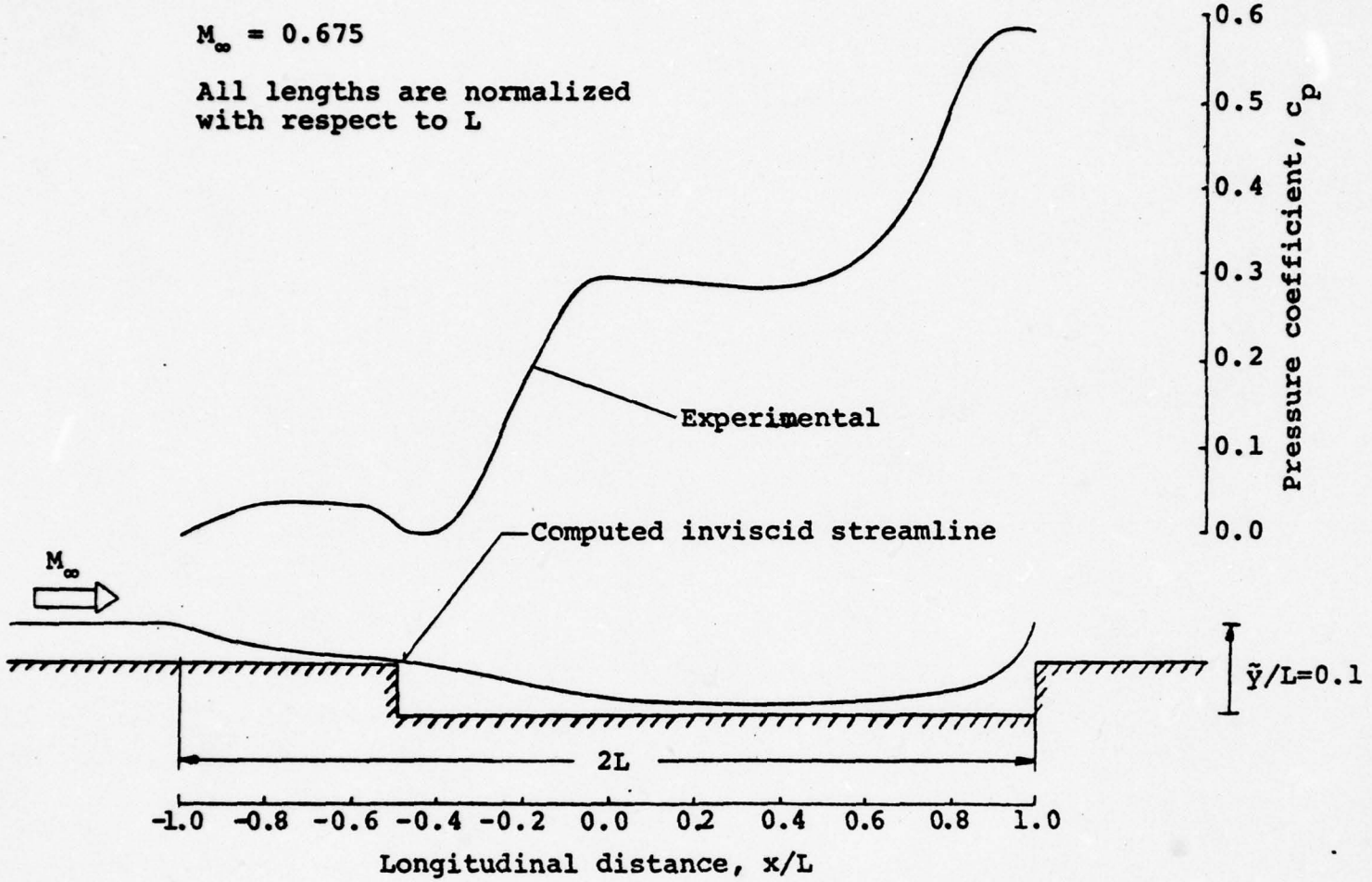

FIGURE 3. Experimental Pressure Coefficient and Computed Streamline For A Shallow Cut Out

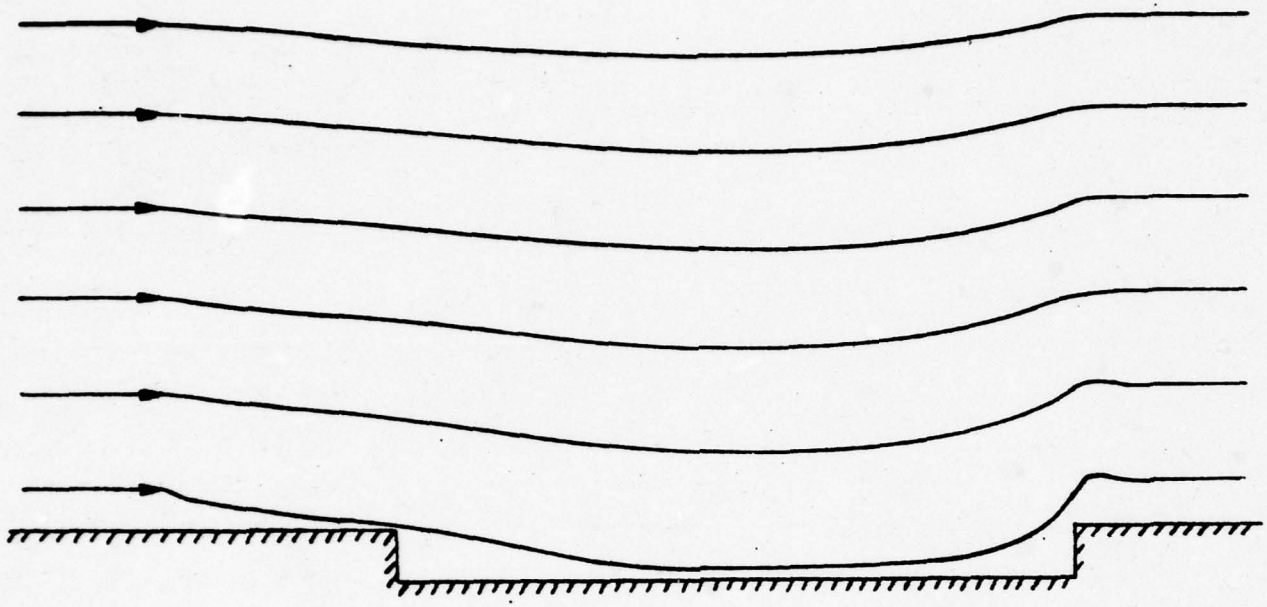

FIGURE 4. Computed Streamlines

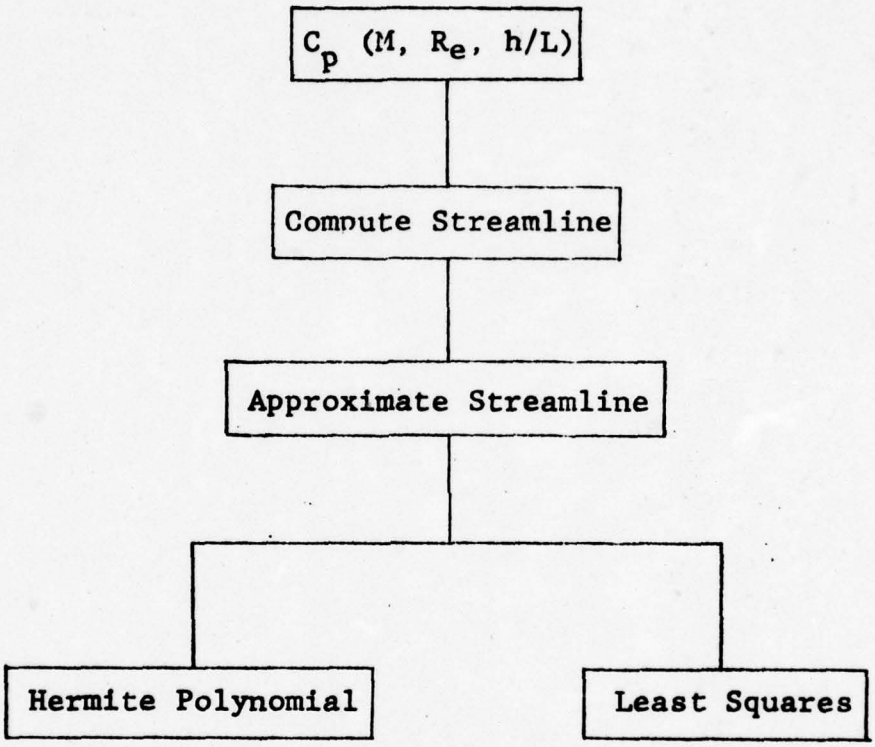

FIGURE 5. Formulation for Streamline Computation

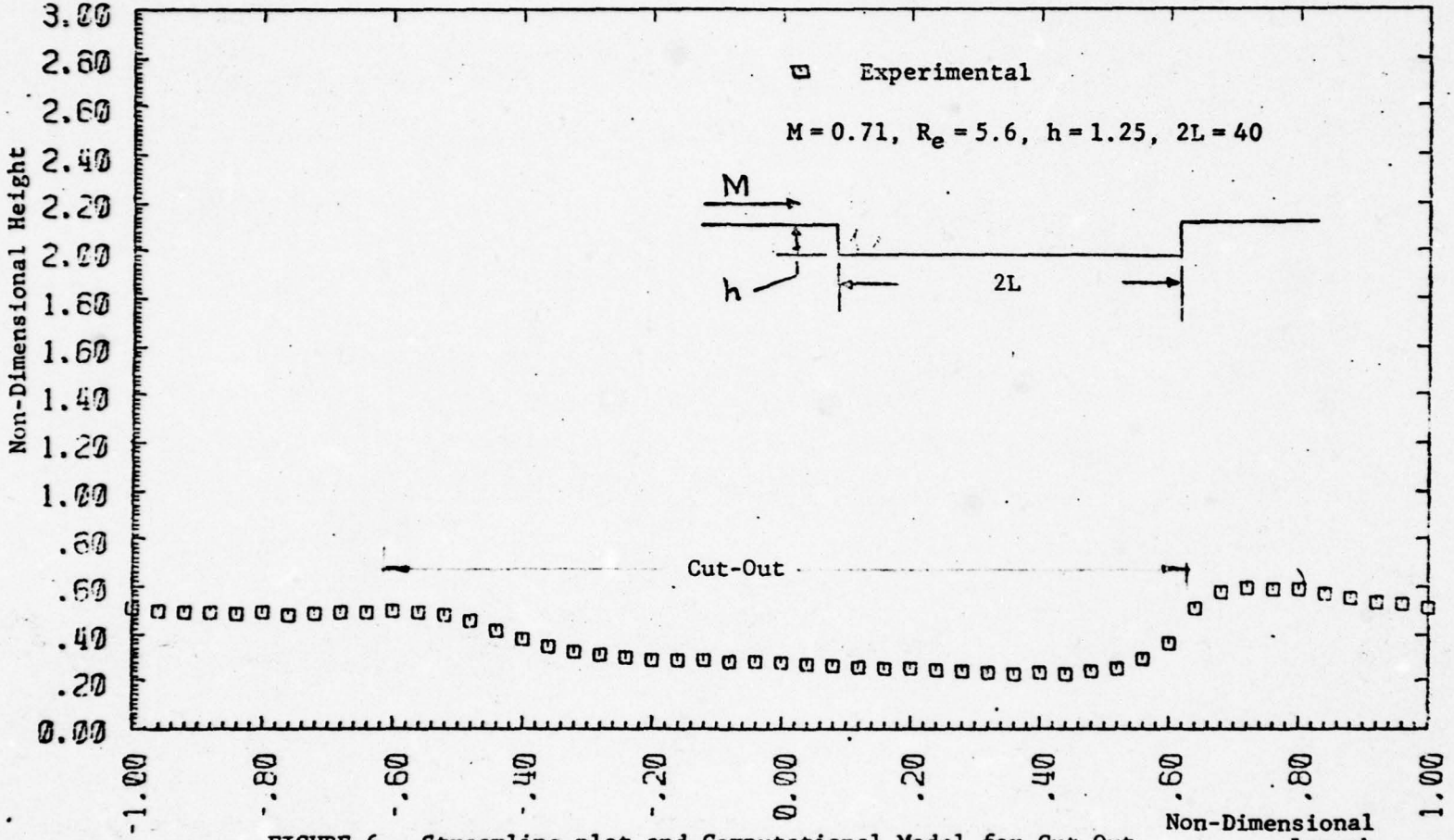

FIGURE 6. Streamline plot and Computational Model for Cut Out

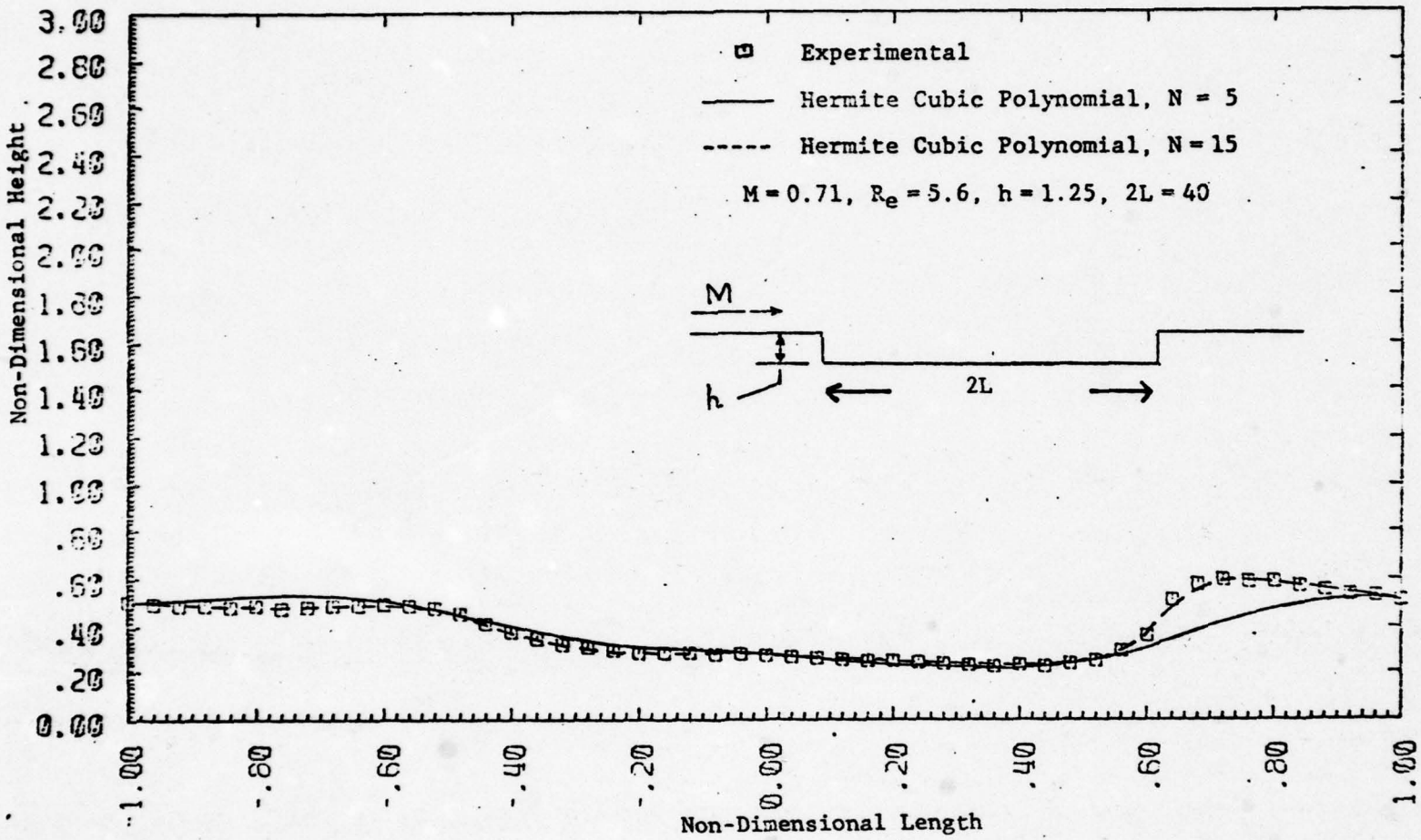

FIGURE 6. (Continued)

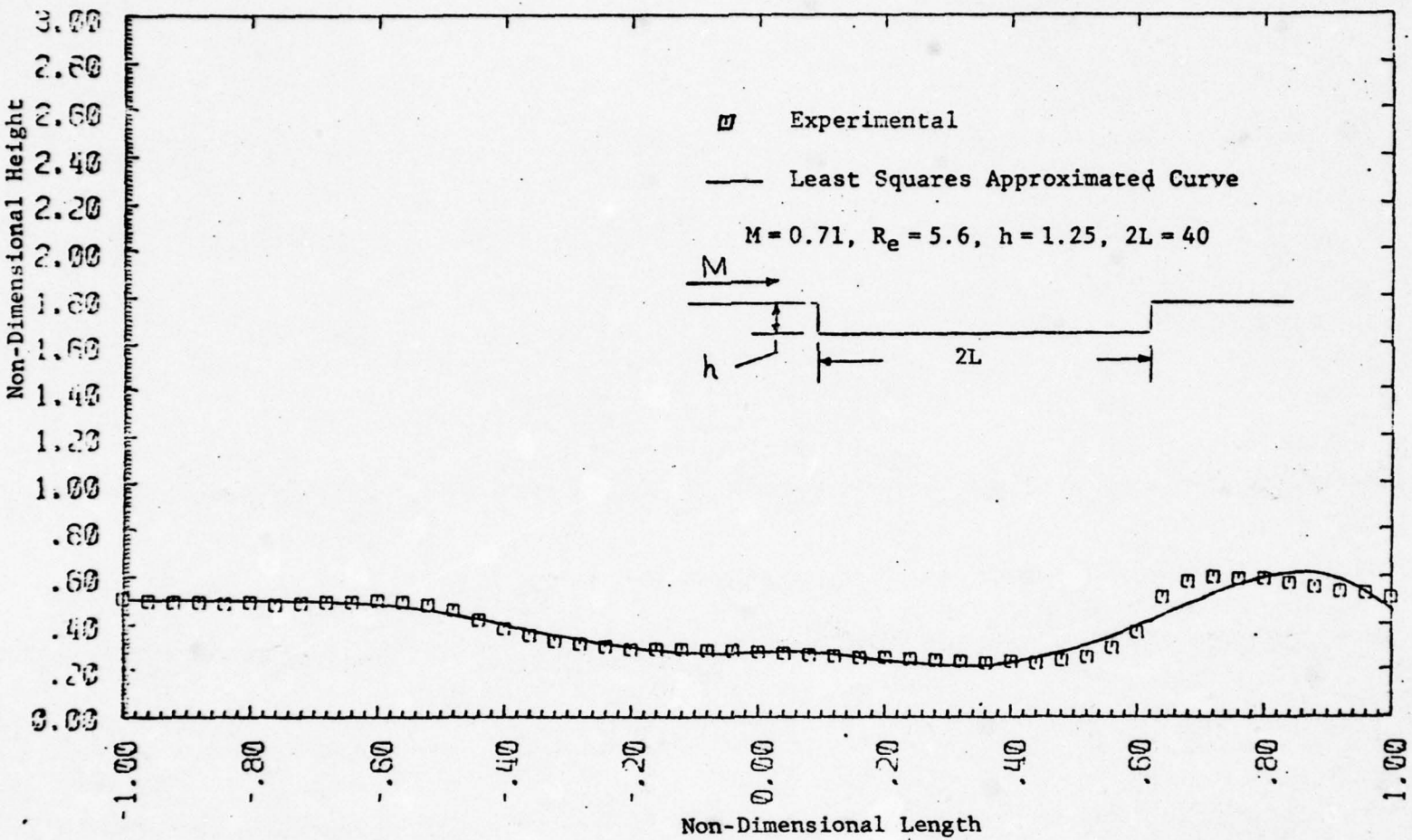

FIGURE 6. (Continued)

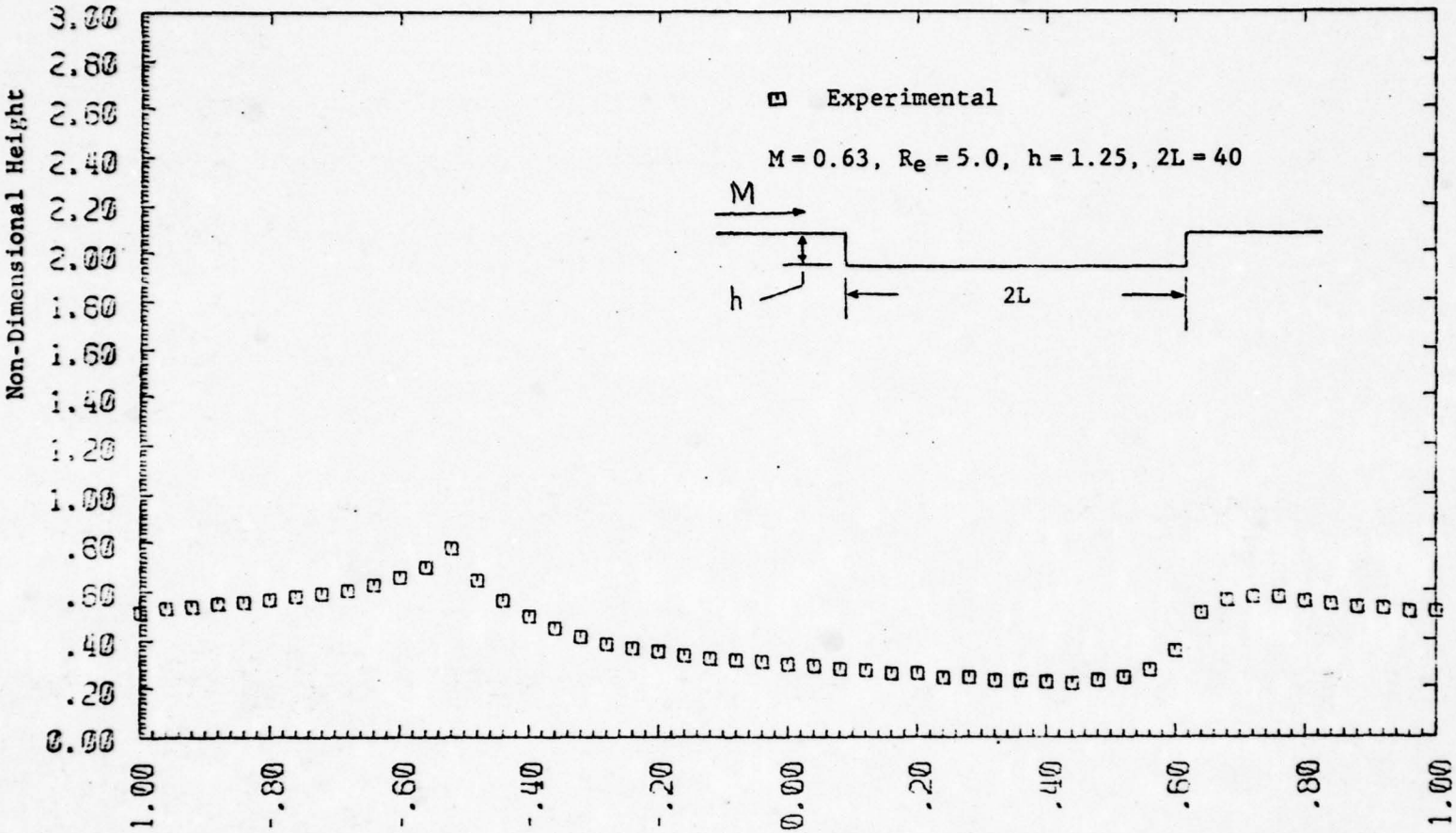

FIGURE 6. (Continued)

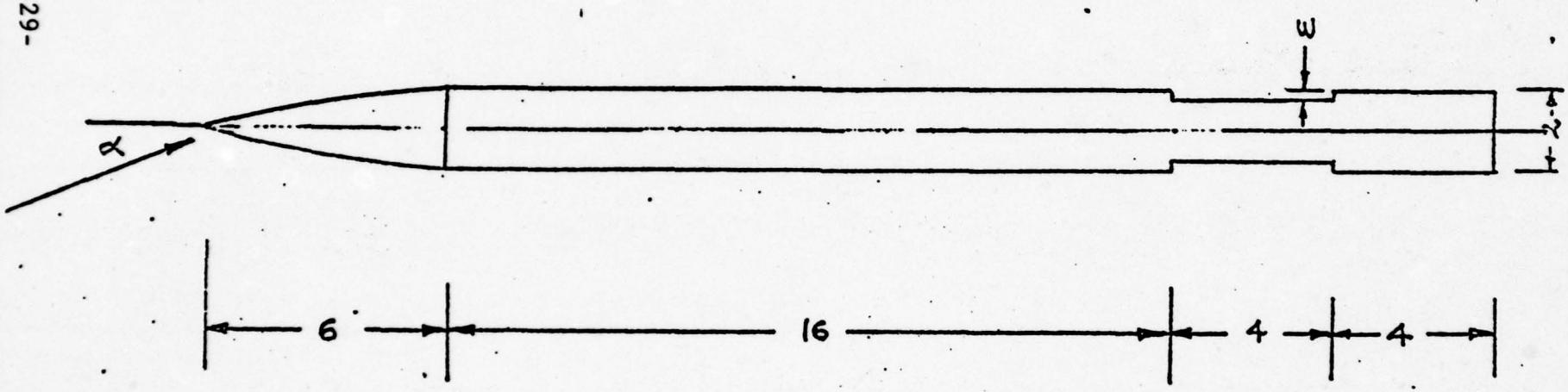

FIGURE 7. Cut Out Configuration For Sample Calculation

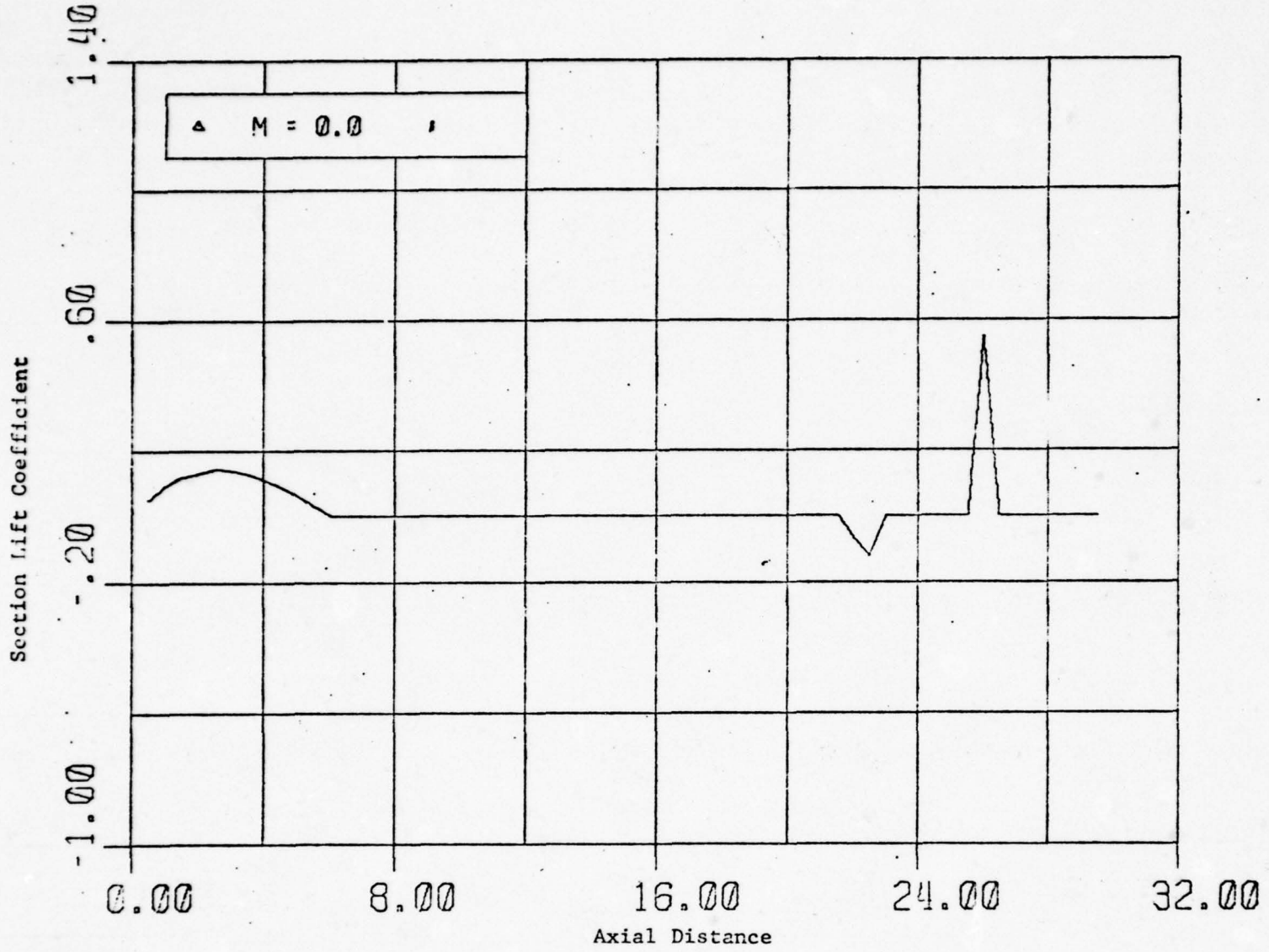

FIGURE 8. Plot of Section Lift Coefficient Along Body Surface

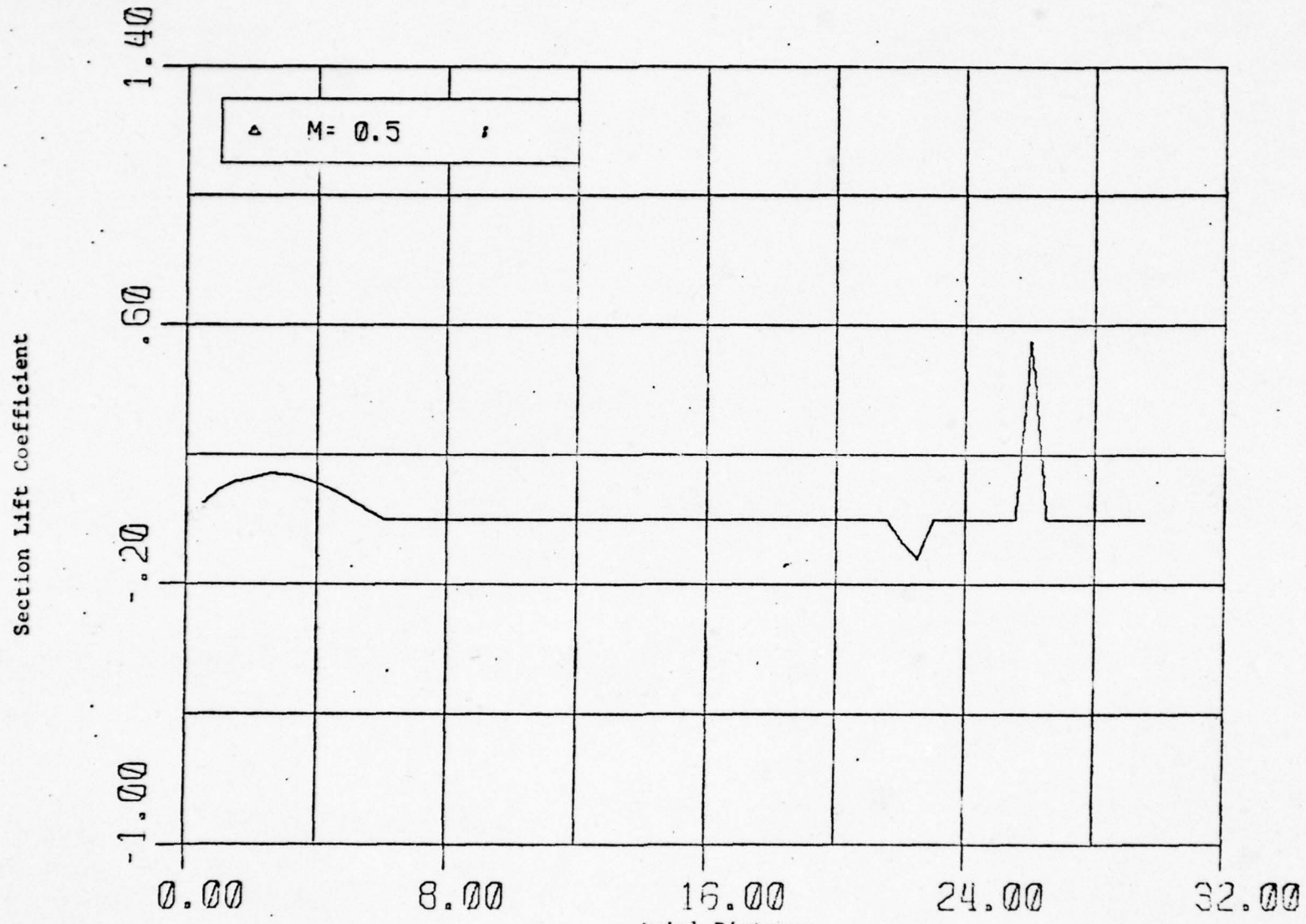

FIGURE 8. (Continued)

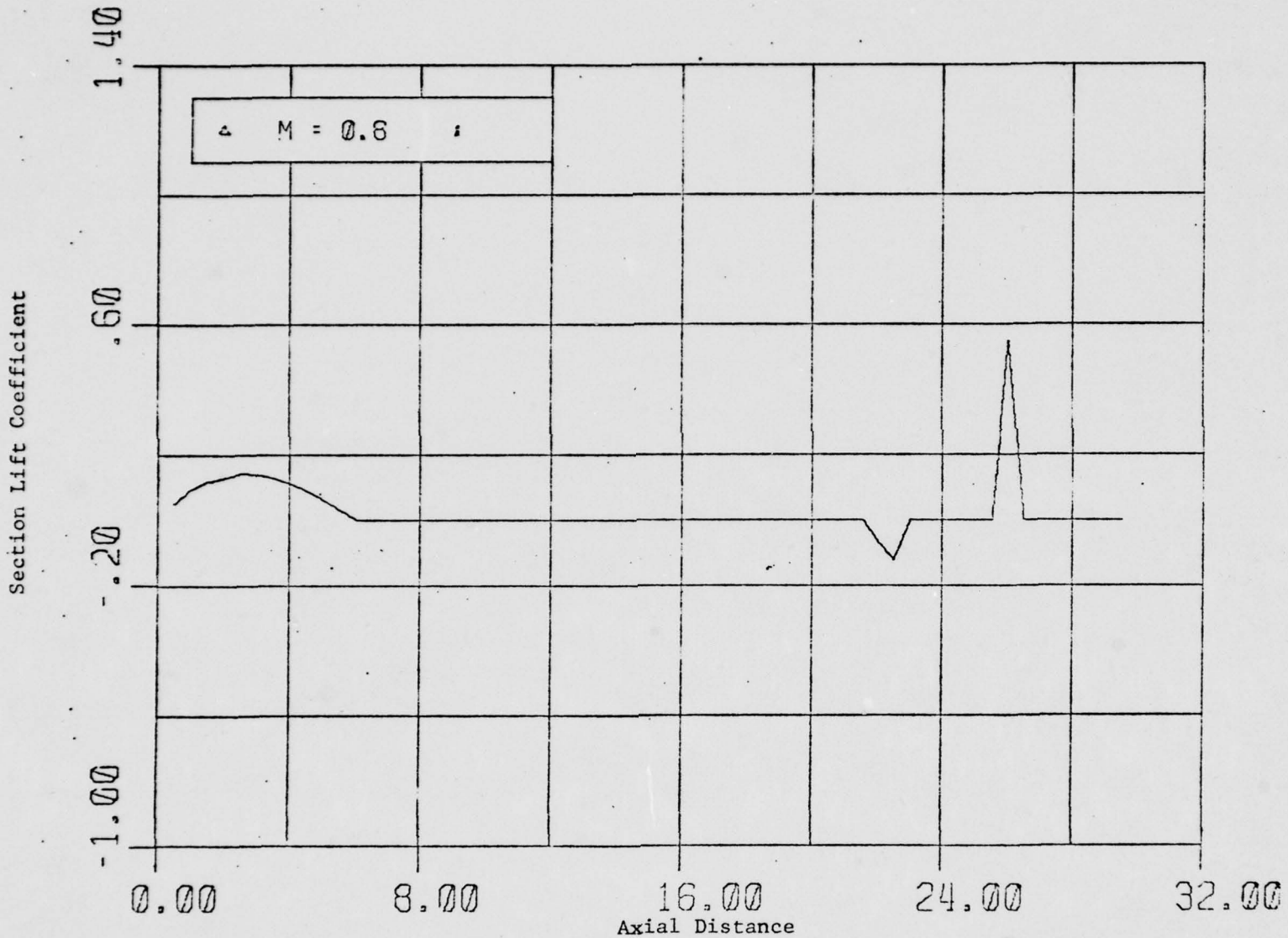

FIGURE 8. (Continued)

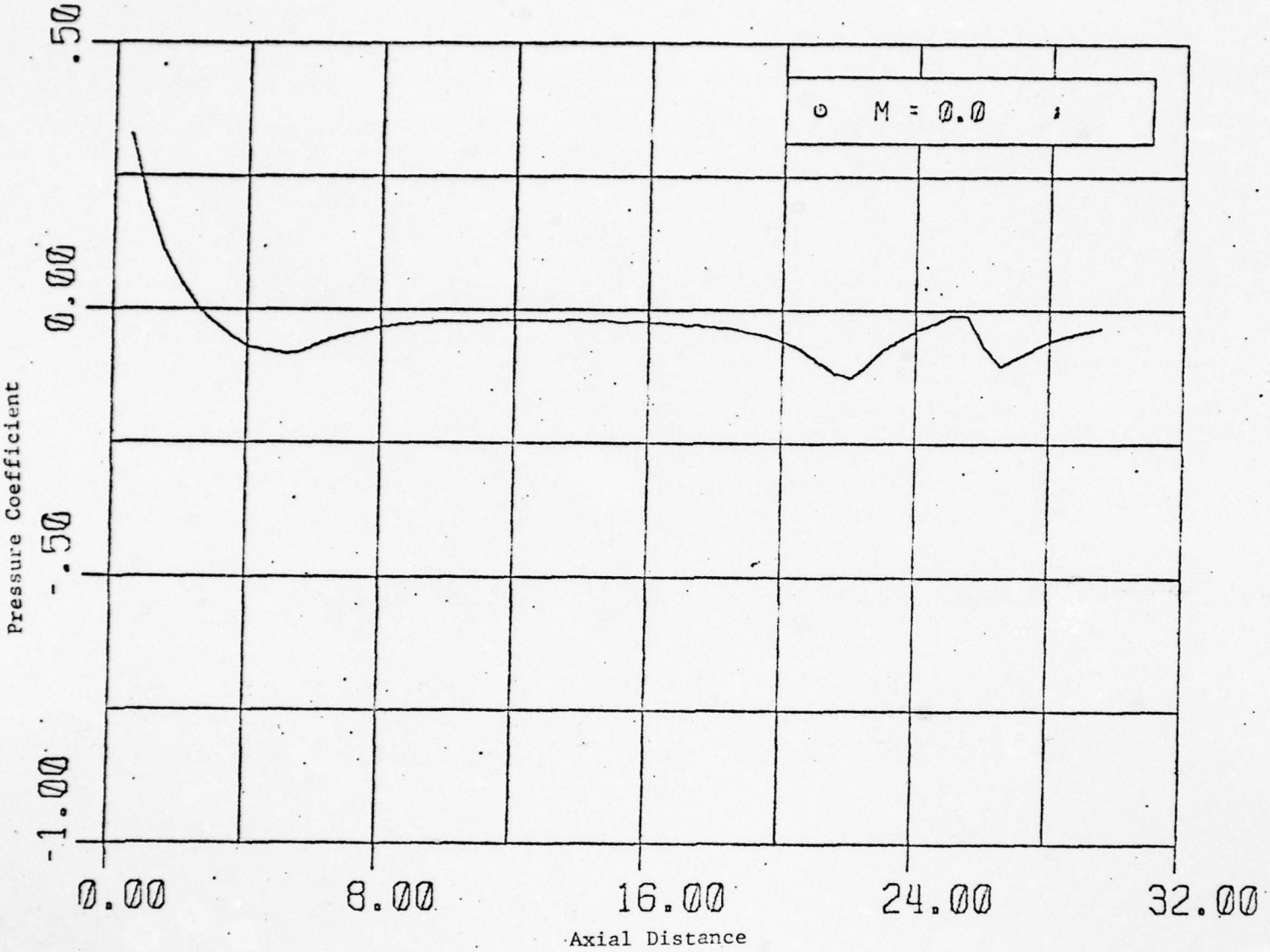

FIGURE 9. Plot of Pressure Coefficient Along Body Surface

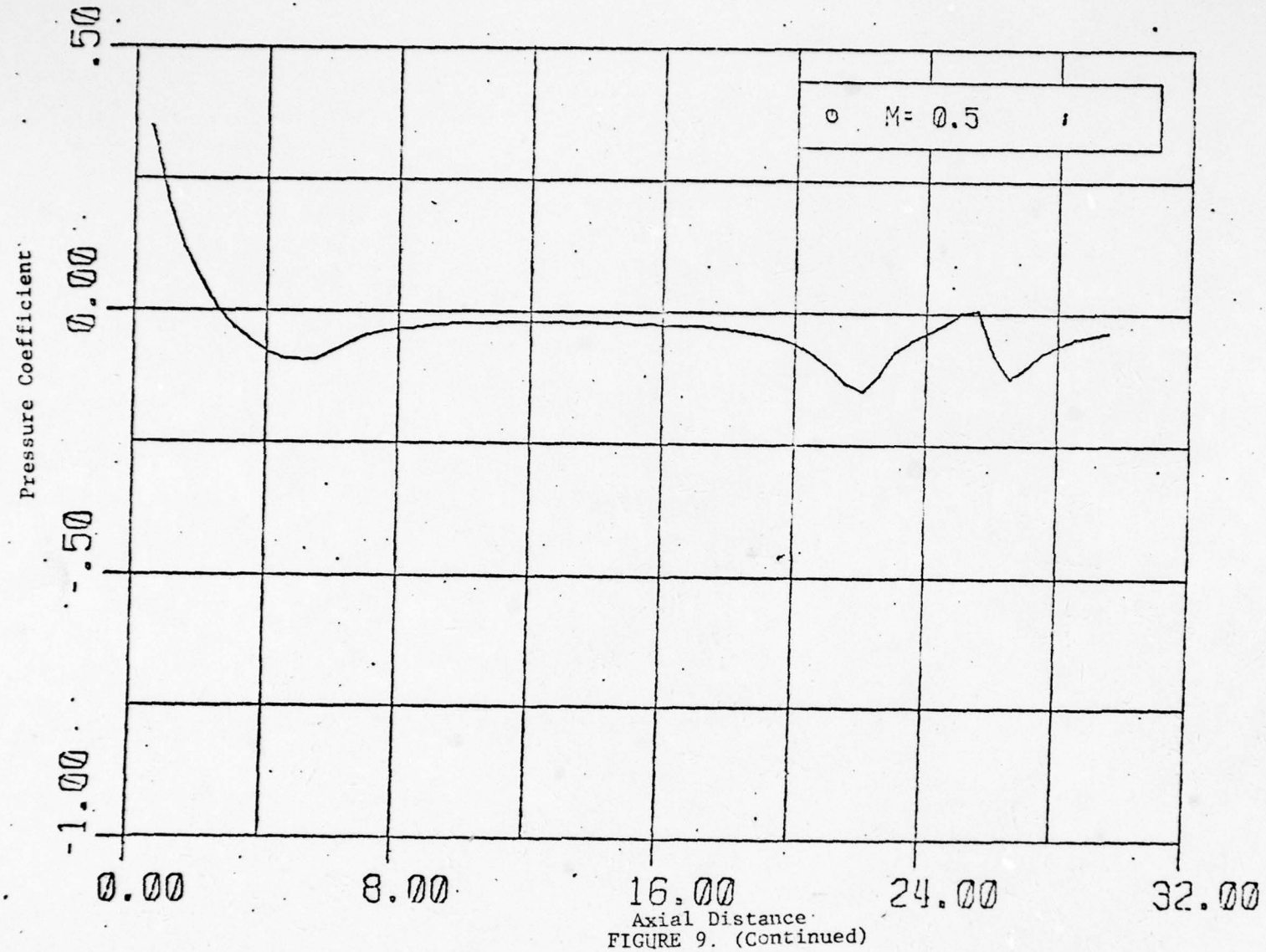

FIGURE 9. (Continued)

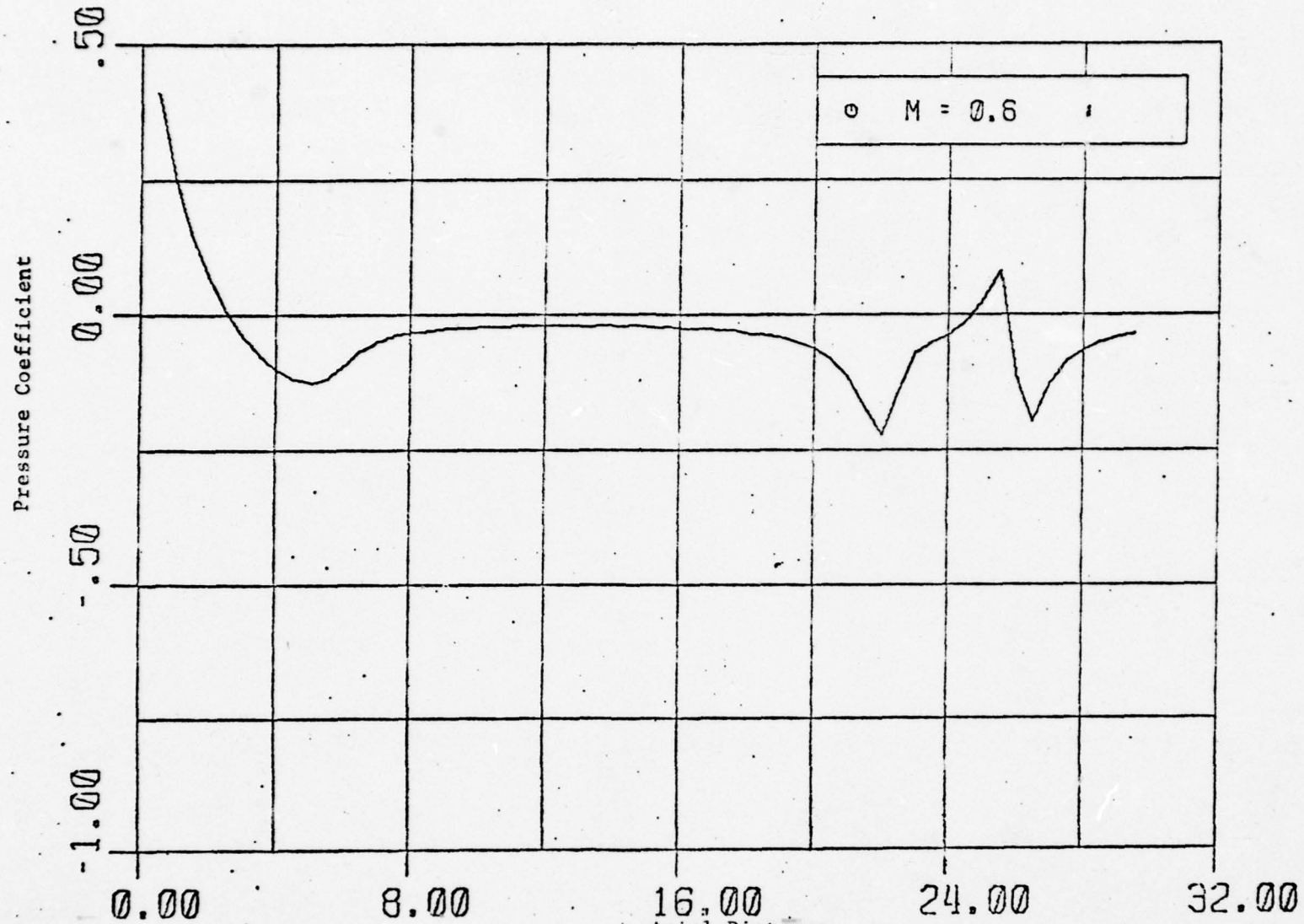

FIGURE 9. (Continued)

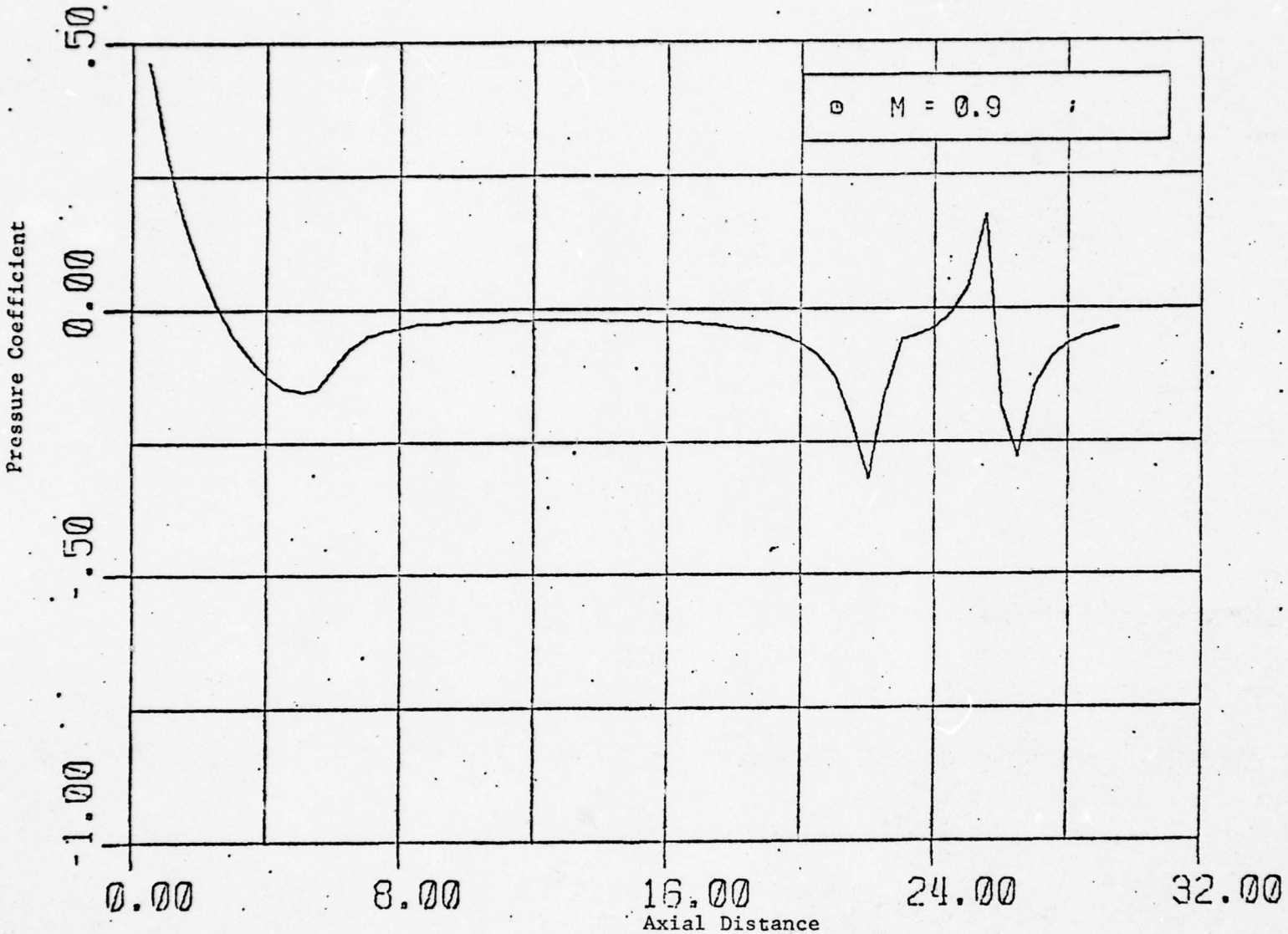

FIGURE 9. (Continued)

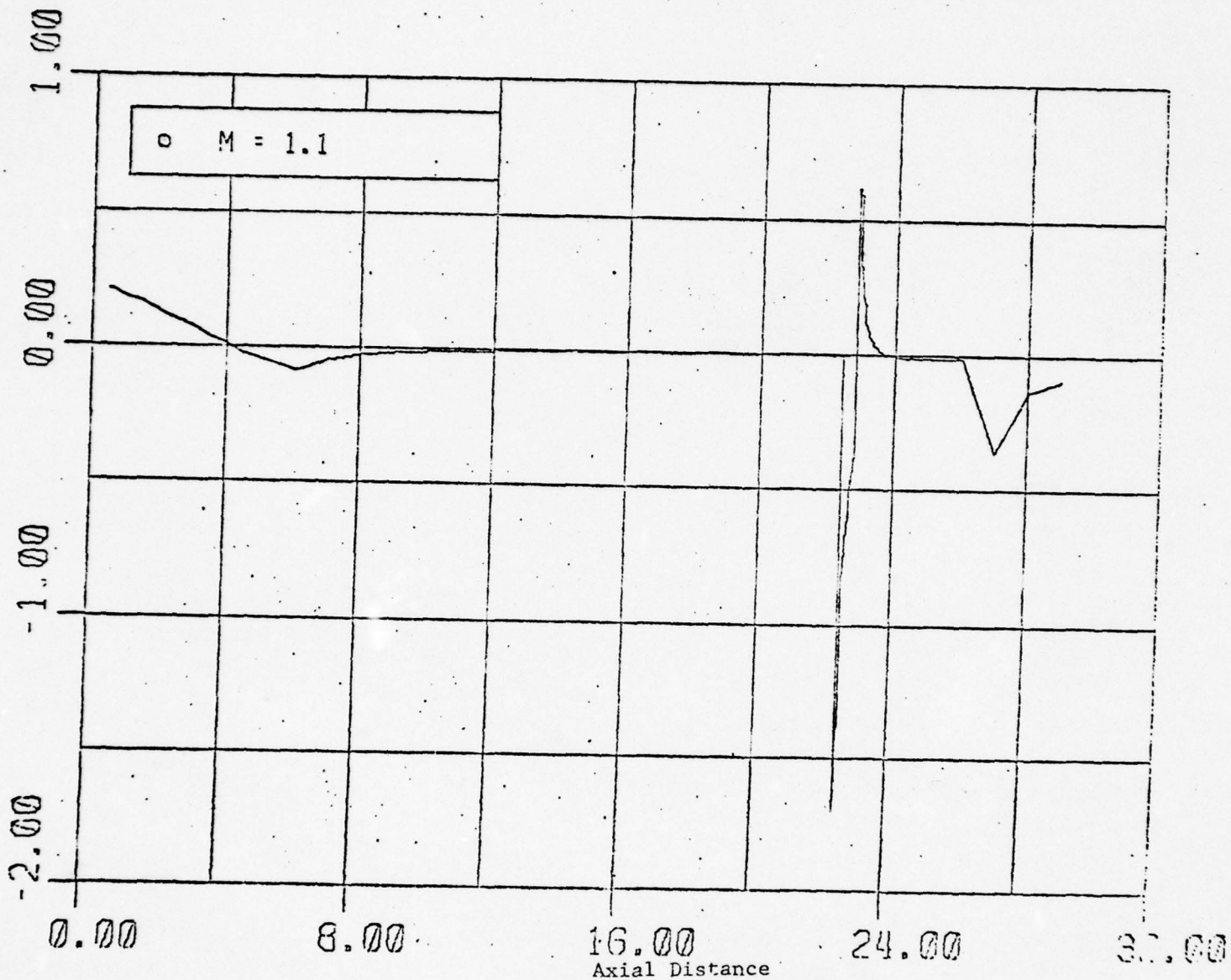

FIGURE 9. (Continued)

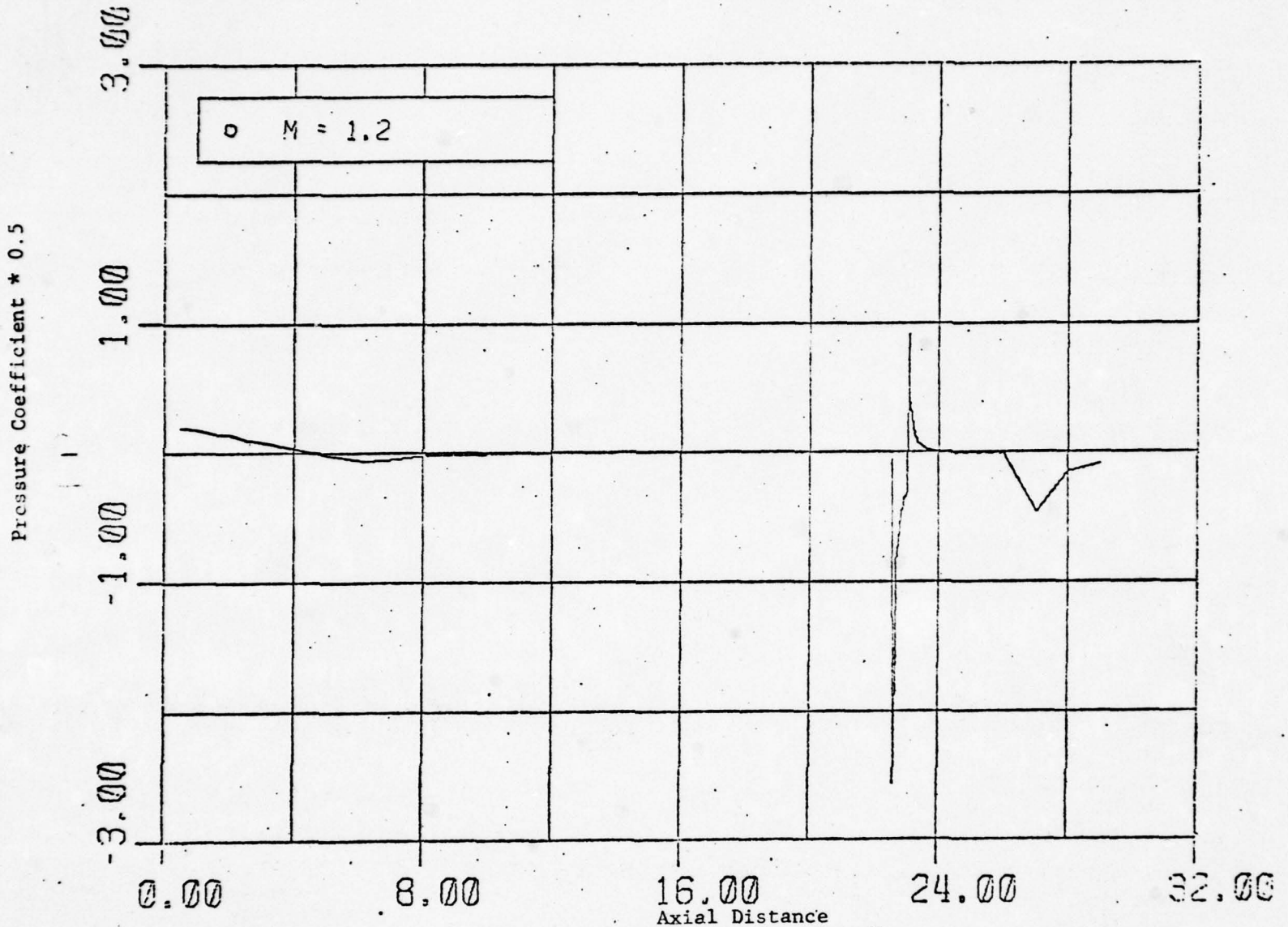

FIGURE 9. (Continued)

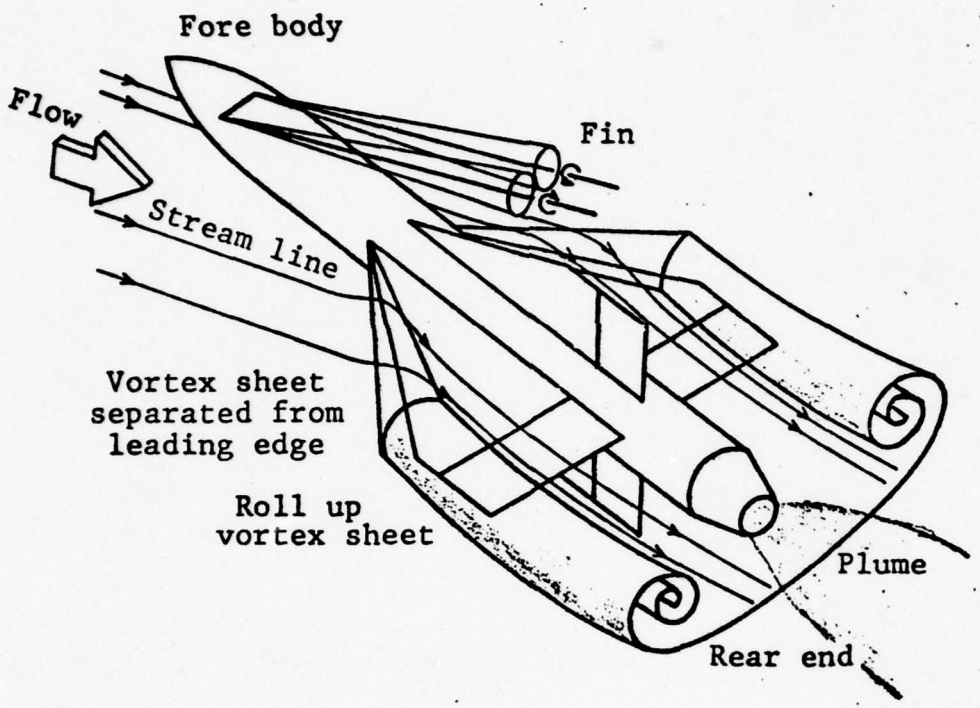

FIGURE 10. Schematic flow field around missile configuration at moderately high angle of attack with emphasis on fin effects.

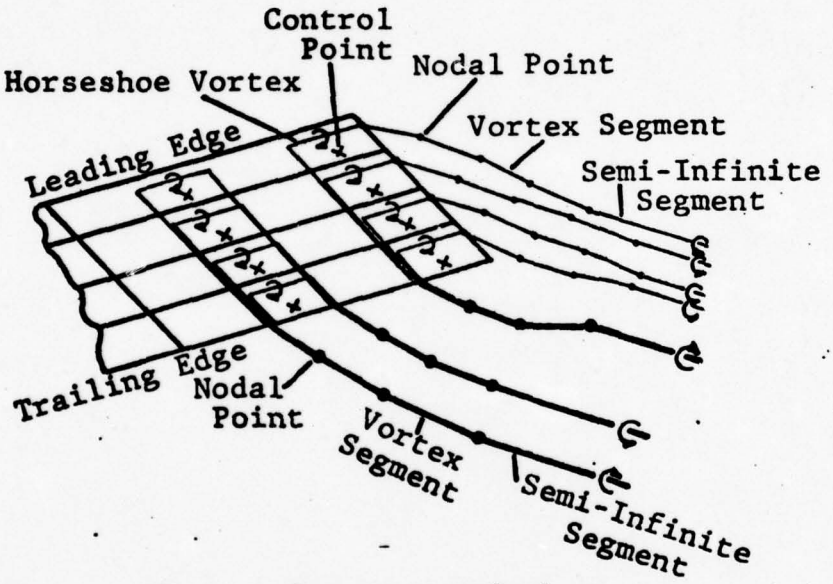

FIGURE 11. Vortex lattice method at high angle of attack.

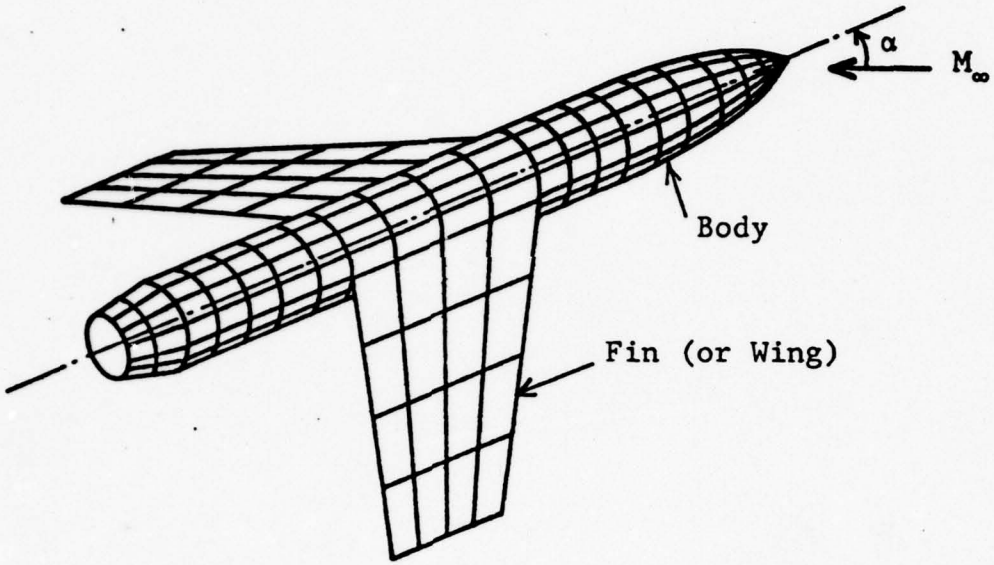

FIGURE 12. Schematic model of a fin-body combination in the present analysis with an exaggerated fin-body combination.

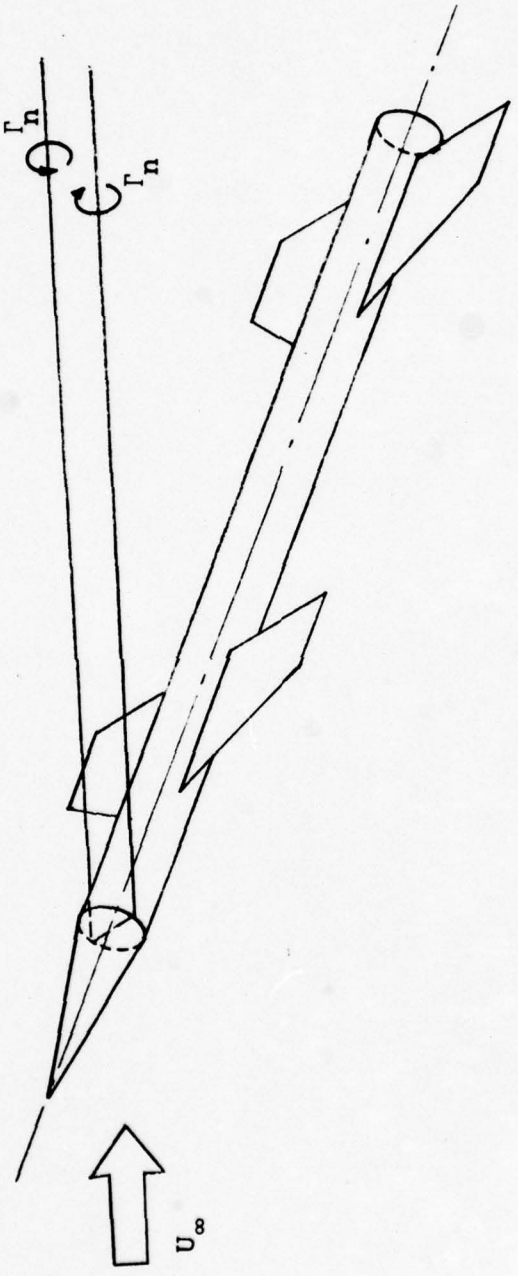

FIGURE 13. Representation of the nose vortex system.

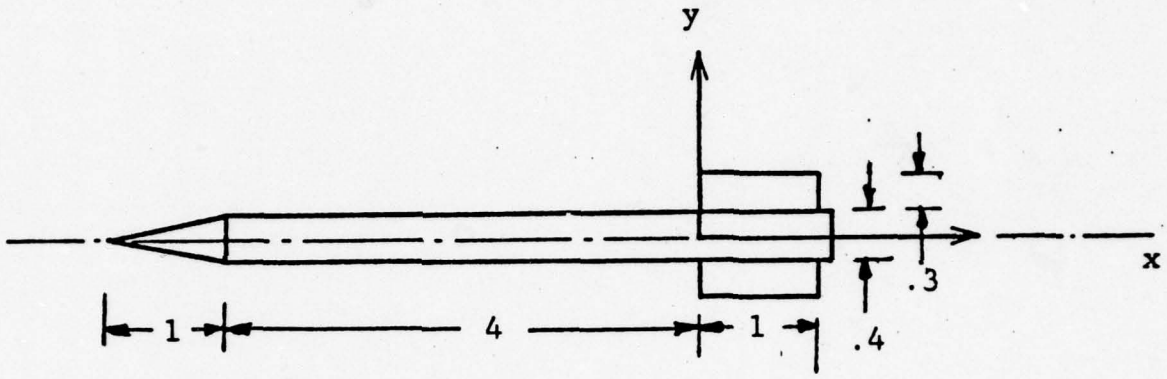

FIGURE 14. Configuration I.

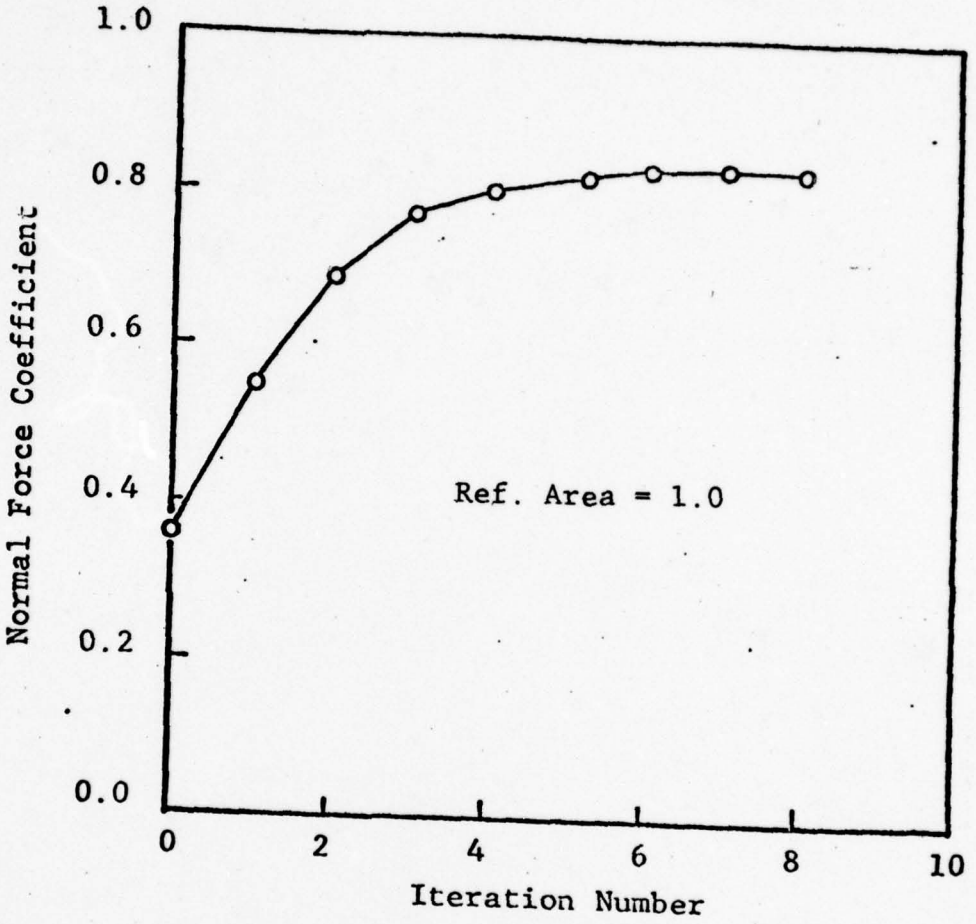

FIGURE 15. Variation of C_N with iteration number (configuration).

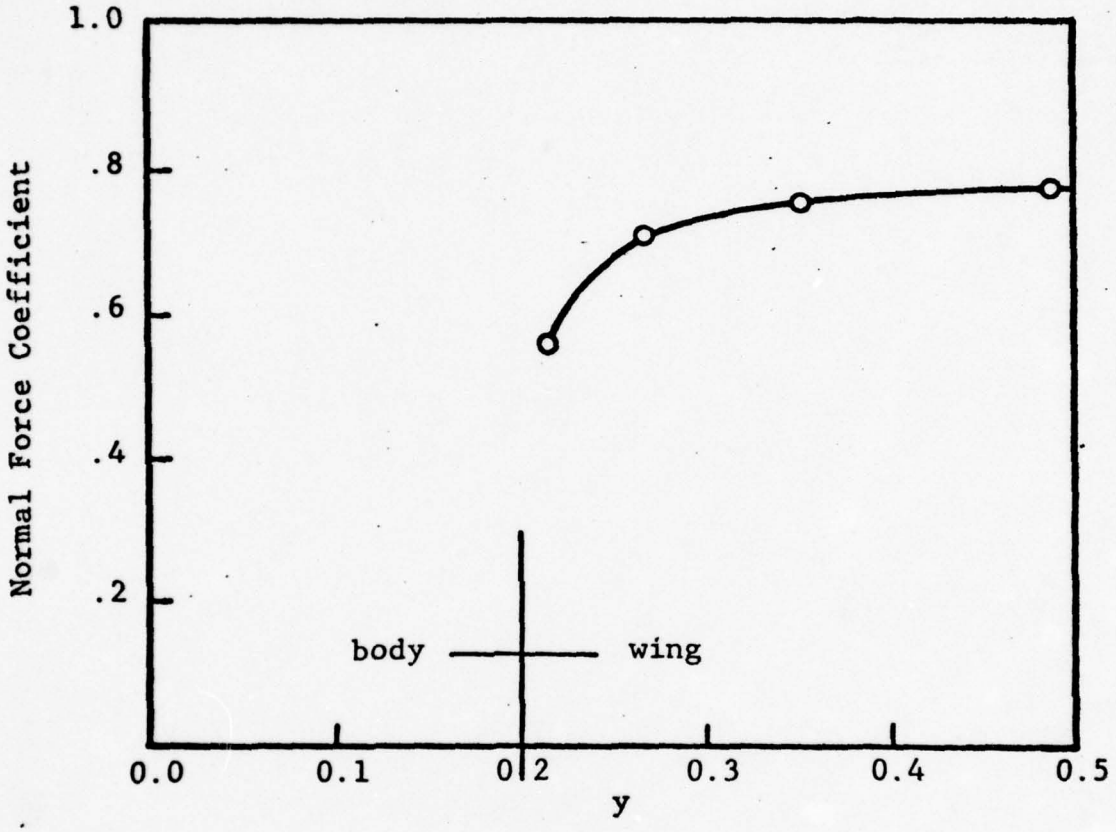

FIGURE 16. Spanwise lift distribution (configuration I).

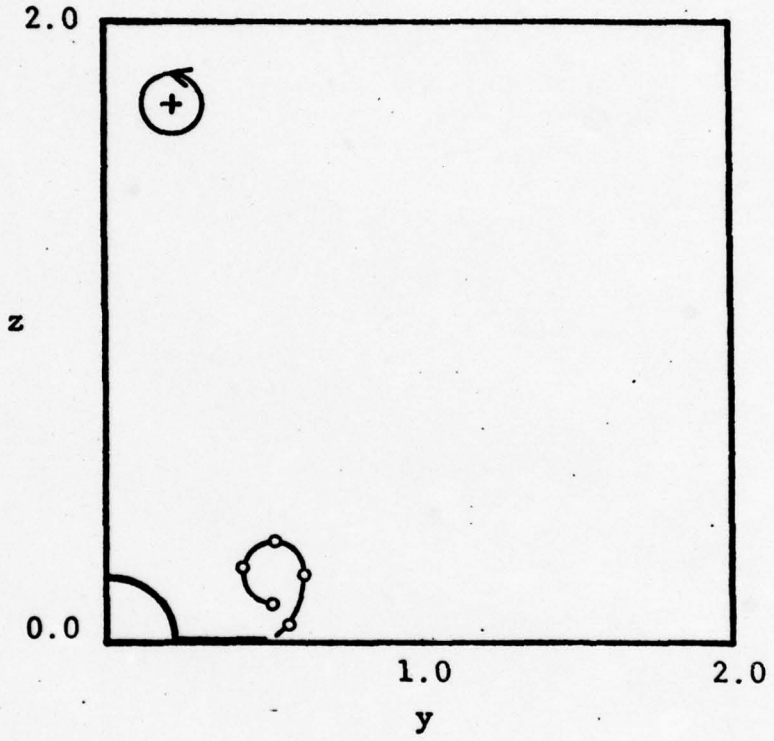

FIGURE 17. Vortex system including nose vortex at x = 1 (configuration I).

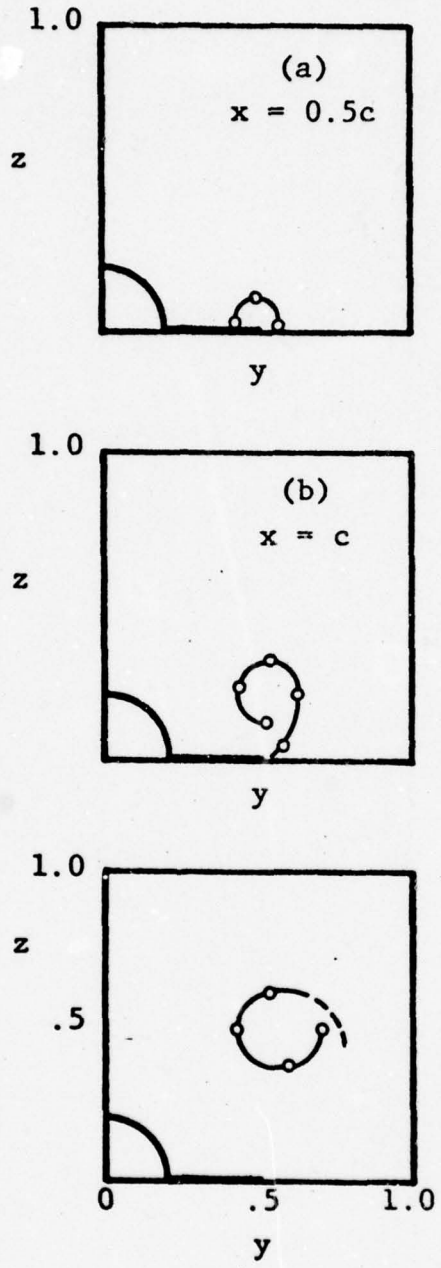

FIGURE 18. Vortex formation on the wing (configuration I).

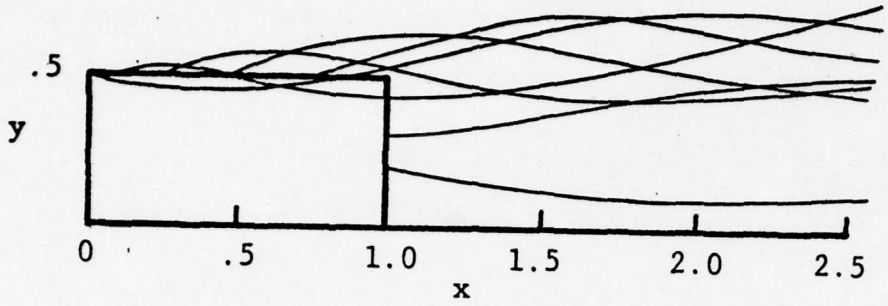

FIGURE 19. Vortex filaments in x-y plane.

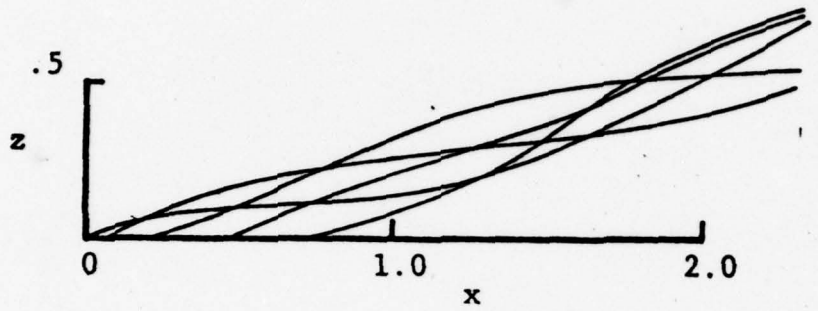

FIGURE 20. Vortex filaments in x-z plane.

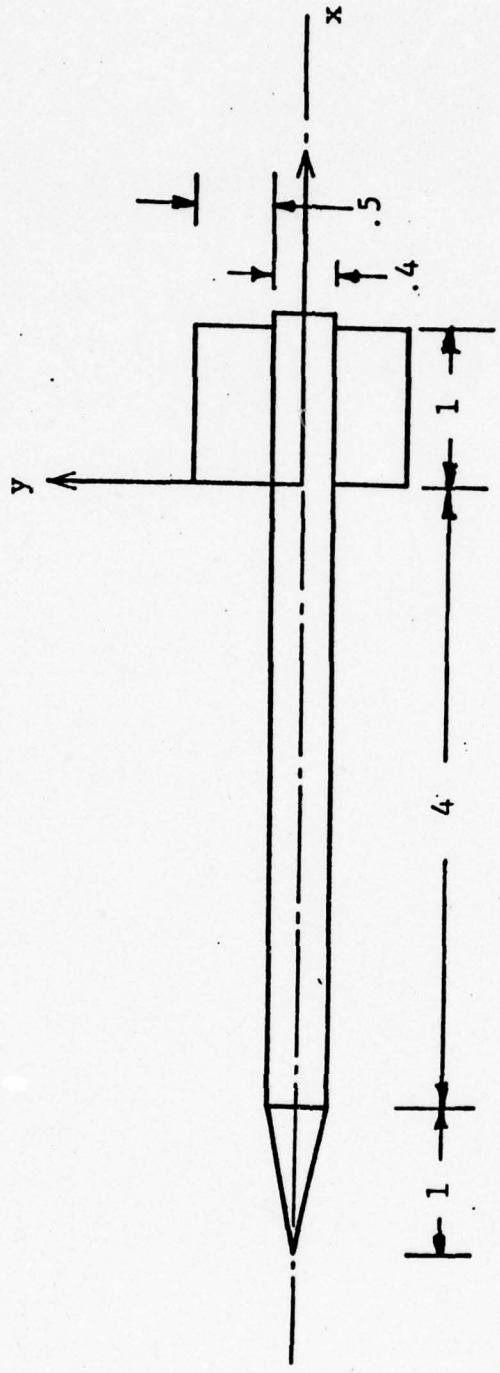

FIGURE 21. Configuration II.

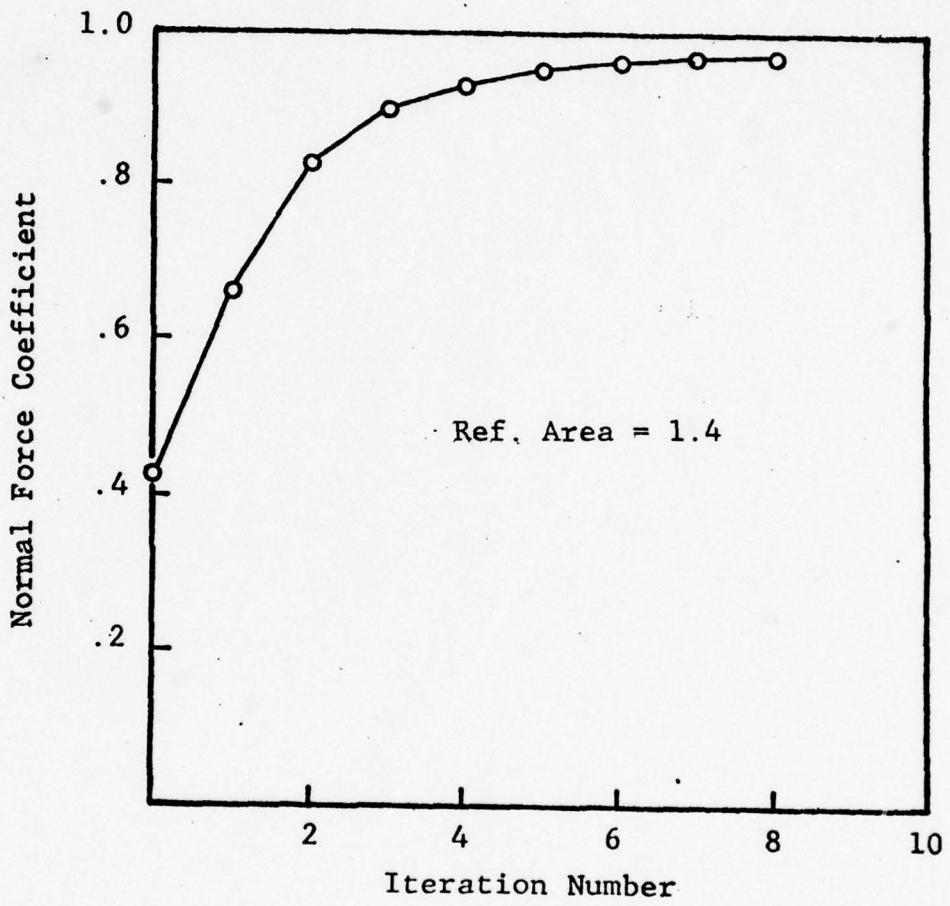

FIGURE 22. Variation of C_N with iteration number (configuration II).

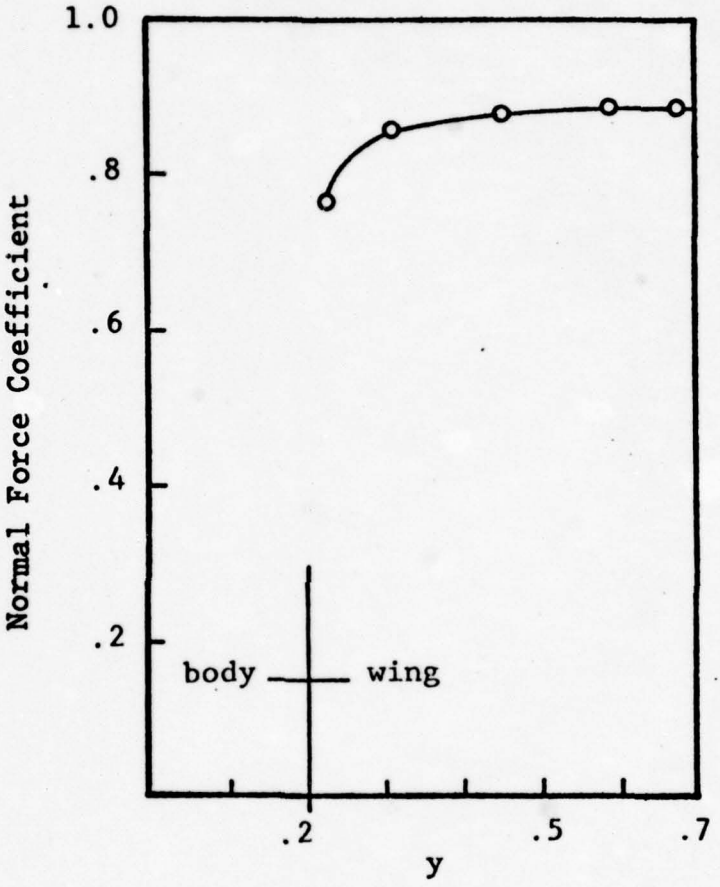

FIGURE 23. Spanwise Load Distribution (Configuration II).

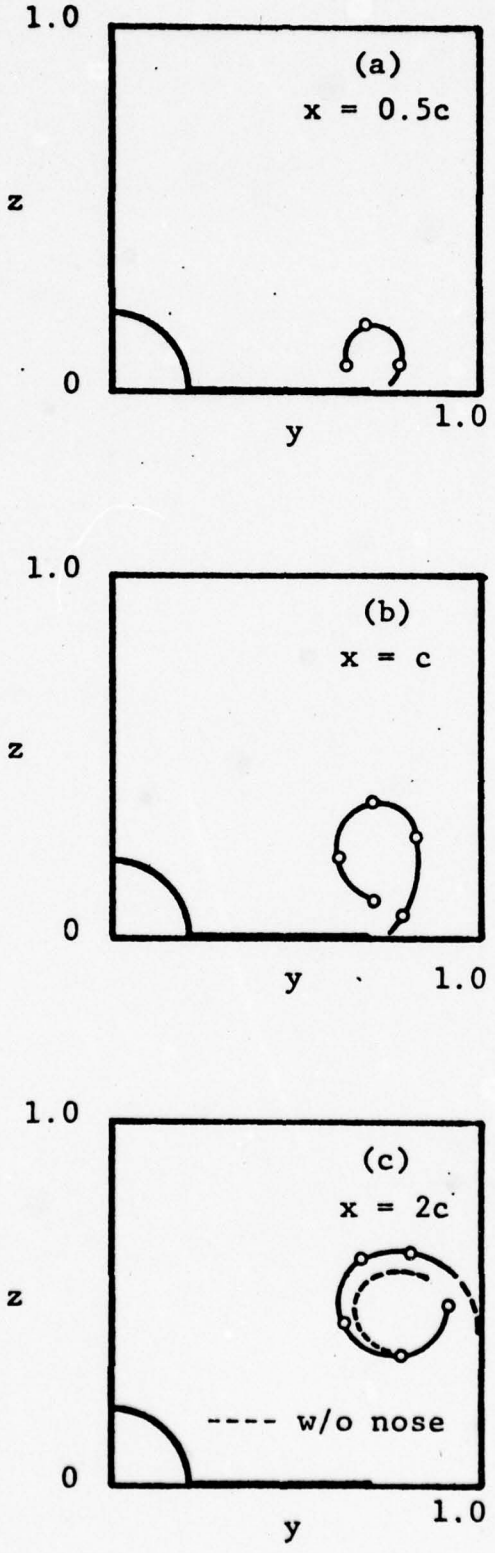

FIGURE 24. Vortex formation on the wing (configuration II).

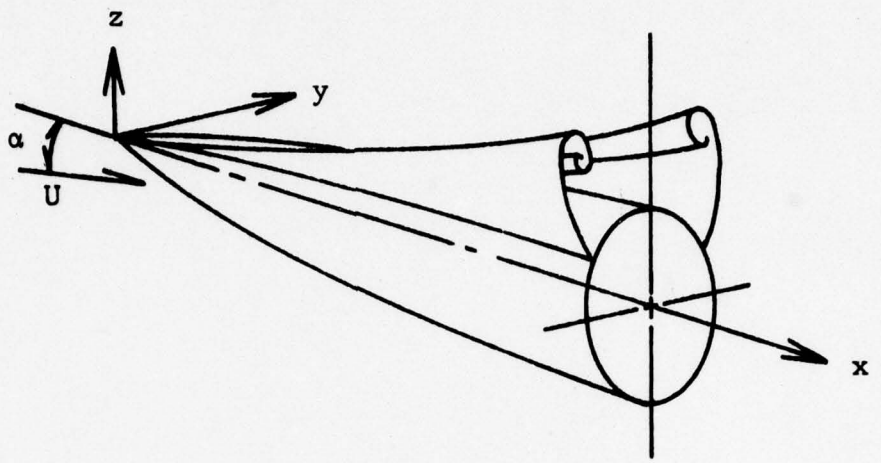

Moderate Angles of Attack of
Symmetric Vortex System

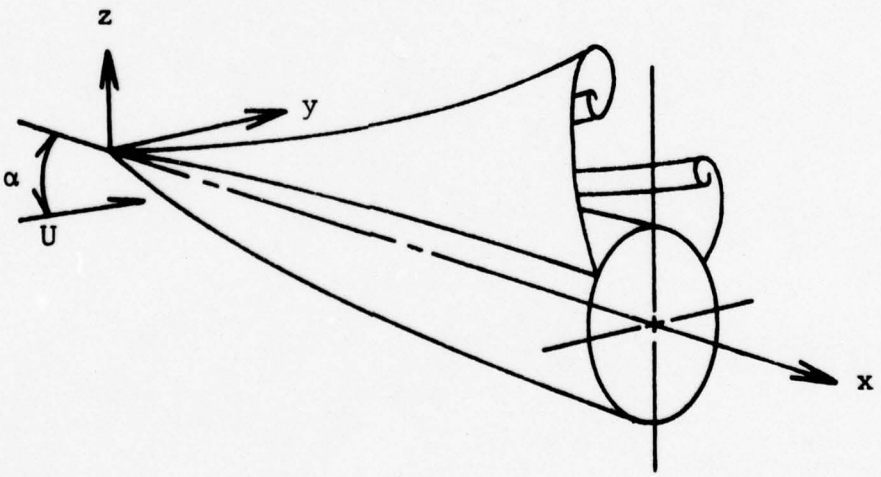

High Angles of Attack of
Asymmetric Vortex System

Figure 25 Schematic and Coordinates of Two Possible Nose Vortex Systems.

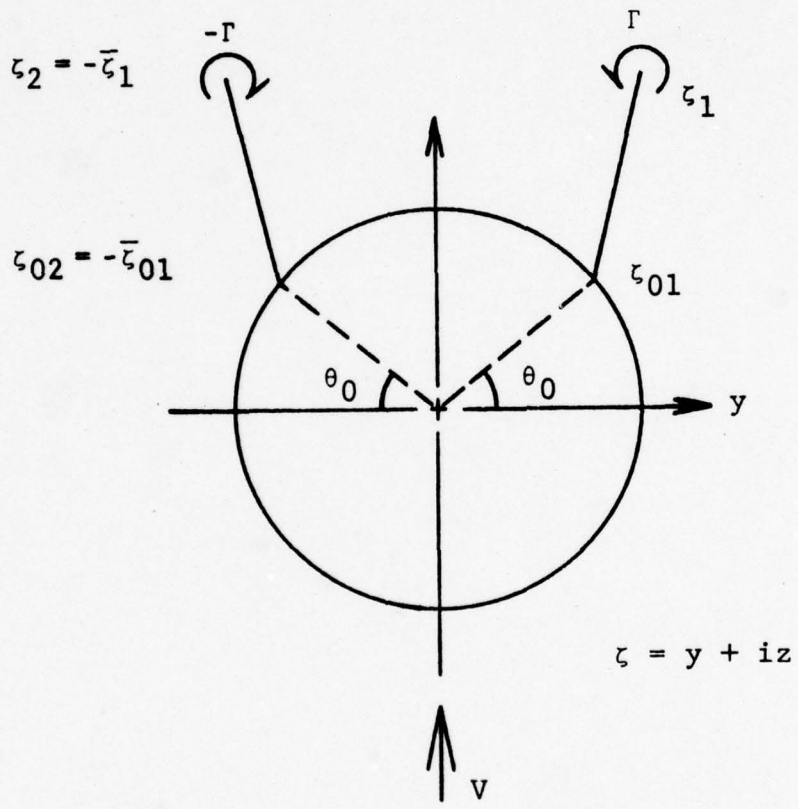

Figure 26. Symmetric Vortex System in a Cross Flow Plane.

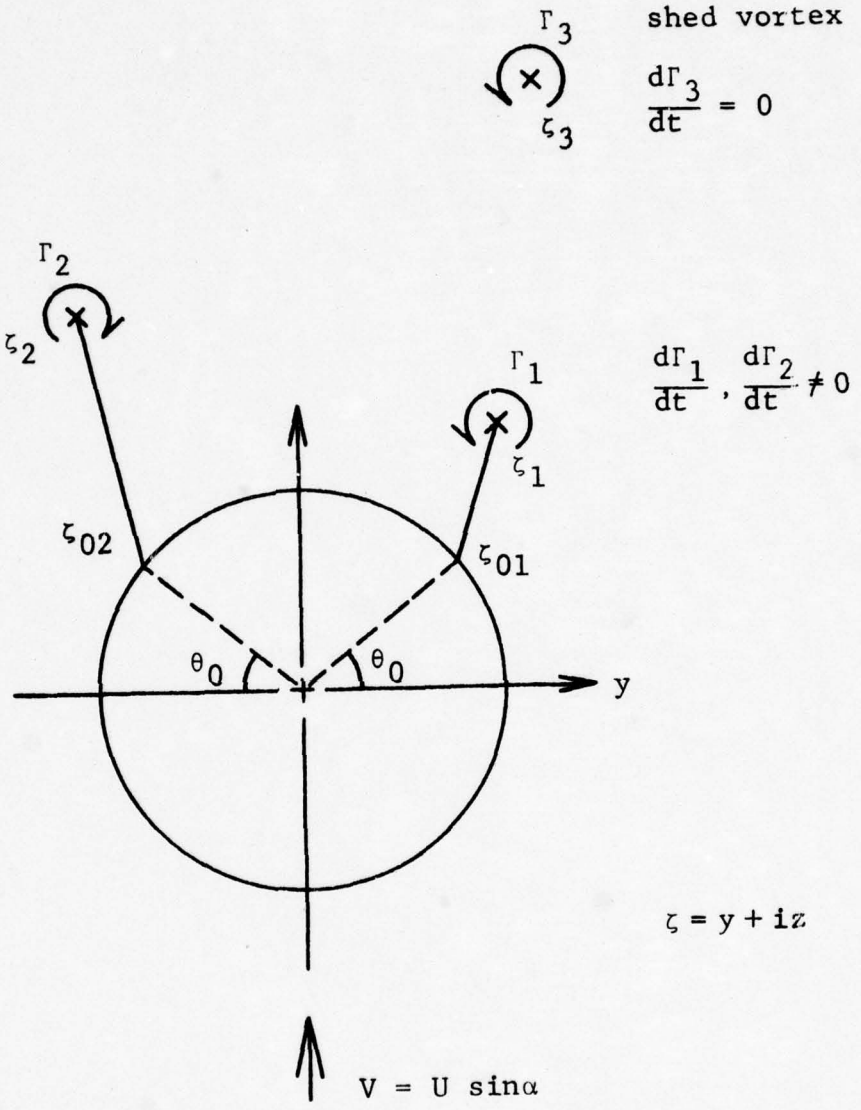

Figure 27. Asymmetric Vortex System in a Cross Flow Plane.

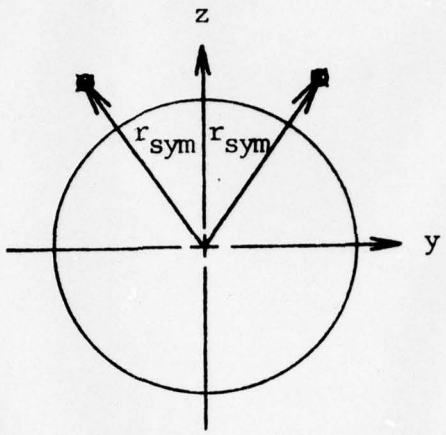

(a) Symmetric Vortices and Before Perturbation

1/2 Asymmetricity

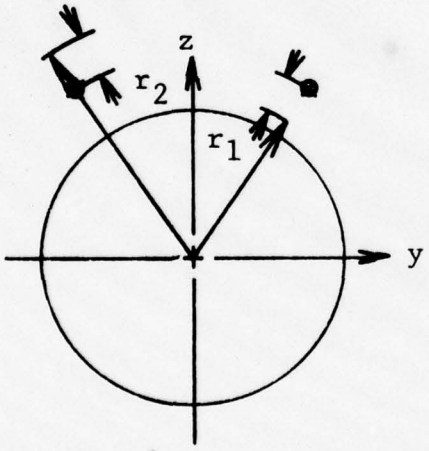

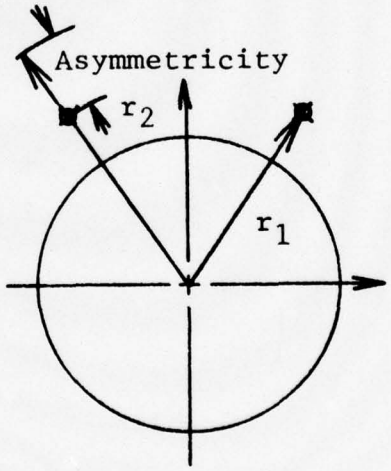

$r_1 = r_{sym} - \frac{1}{2}$ asymmetricity

$r_2 = r_{sym} + \frac{1}{2}$ asymmetricity

Case 1

$r_1 = r_{sym}$

$r_2 = r_{sym}$ + asymmetricity

Case 2

(b) Two Modes of Starting Asymmetric Vortices Pattern

Figure 28. Initial Development of Asymmetricity.

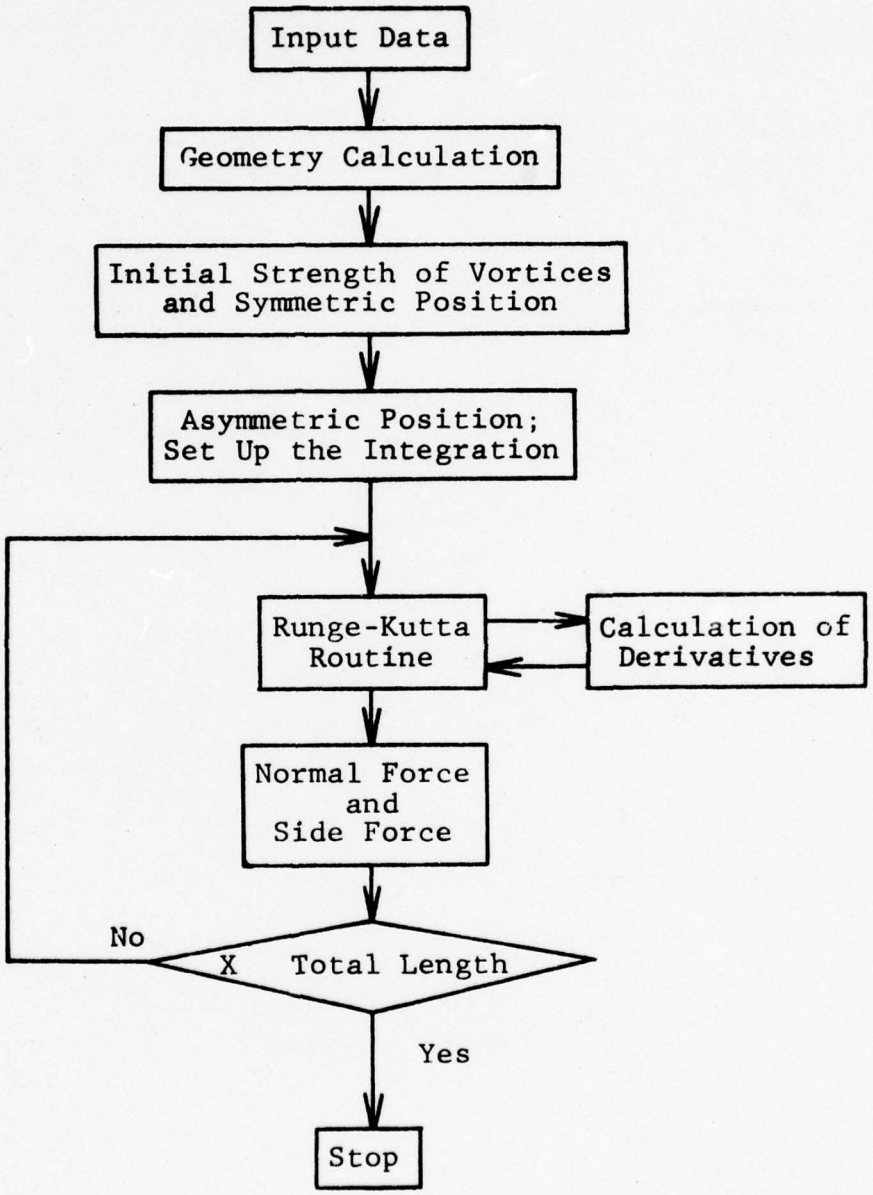

Figure 29. Flow Chart for Numerical Procedures.

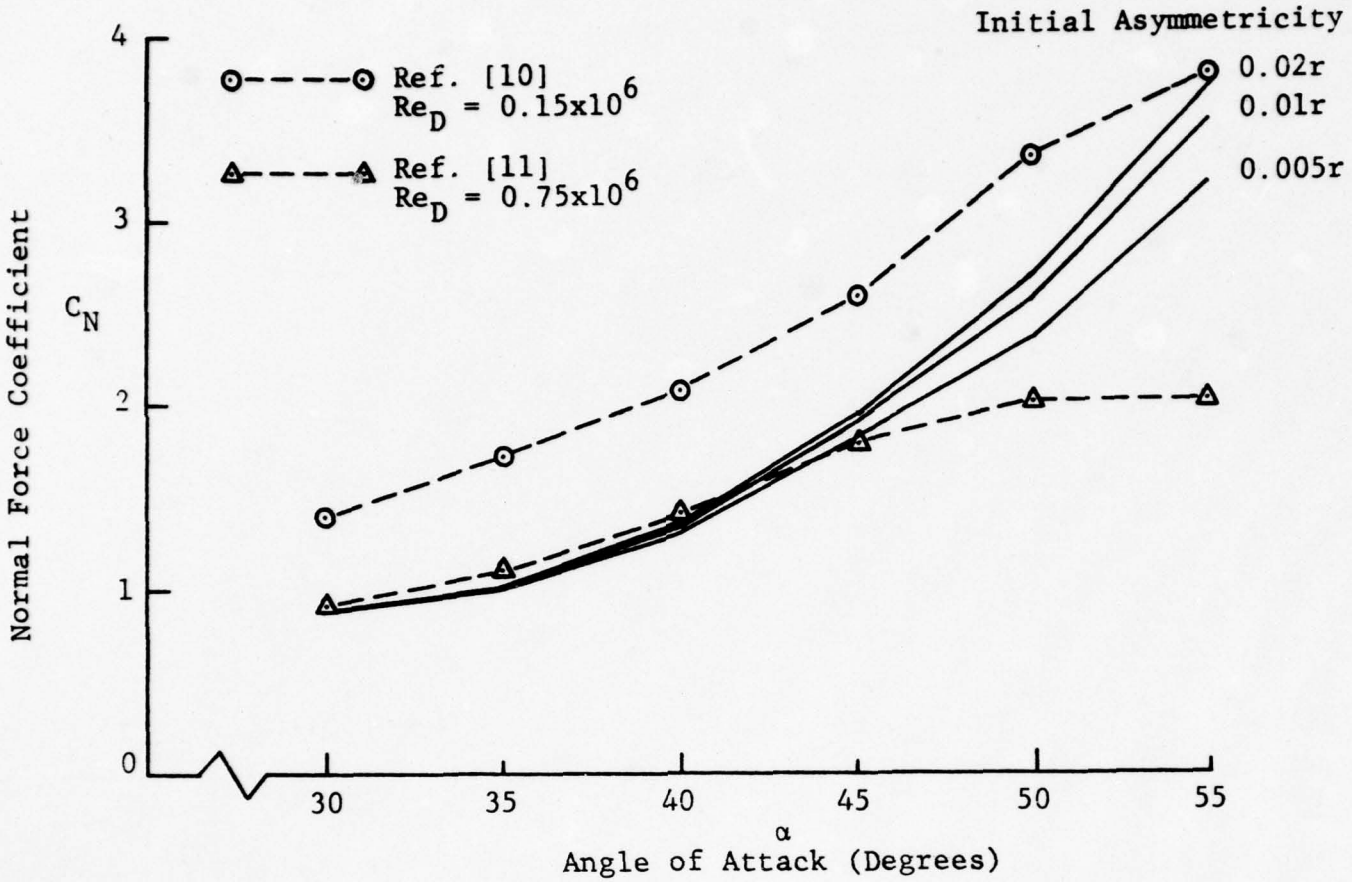

Figure 30. Normal Force Coefficient vs. Angles of Attack for Ogive Forebody (Case 1).

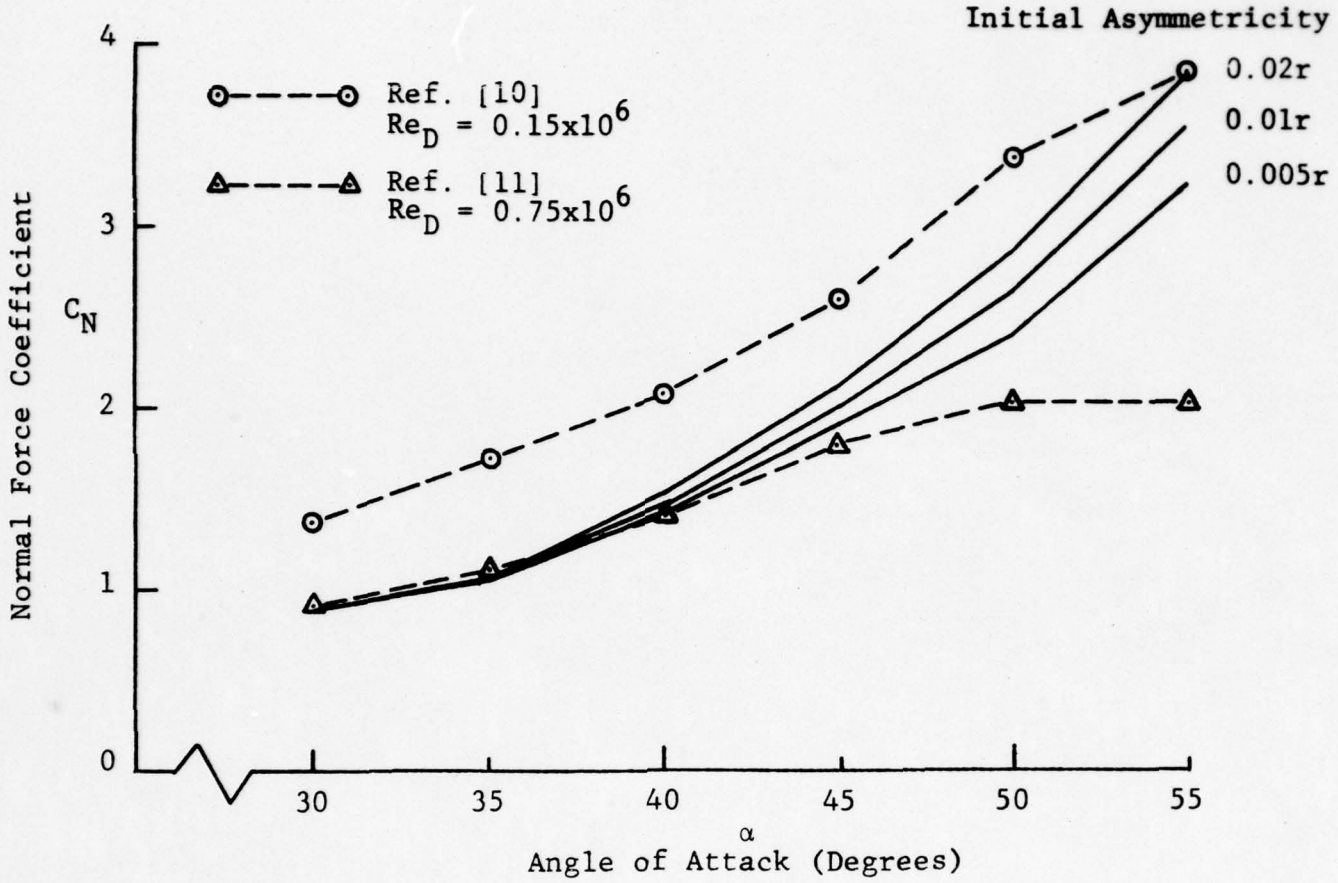

Figure 31. Normal Force Coefficient vs. Angles of Attack for Ogive Forebody (Case 2).

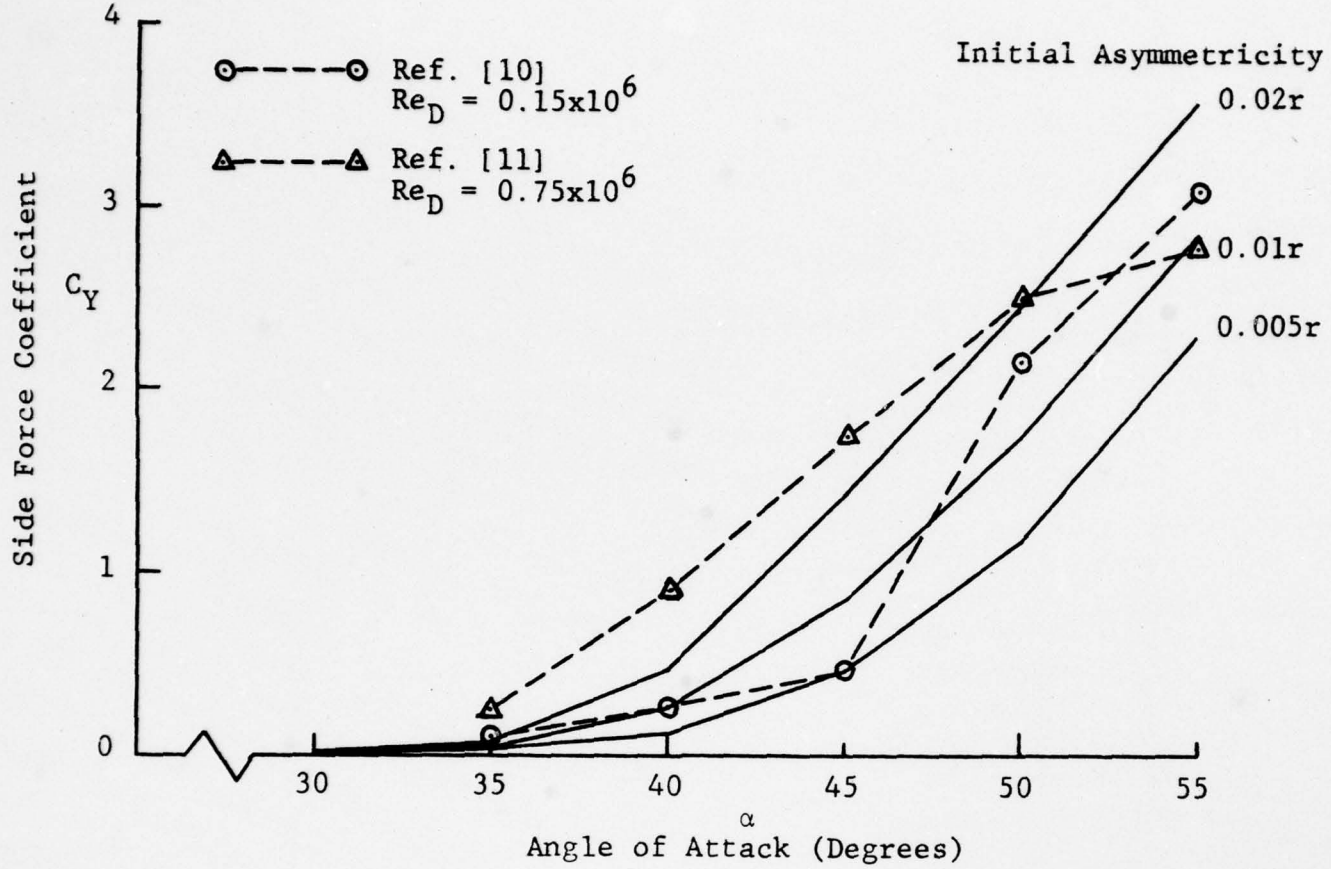

Figure 32. Side Force Coefficient vs. Angles of Attack for Ogive Forebody (Case 1).

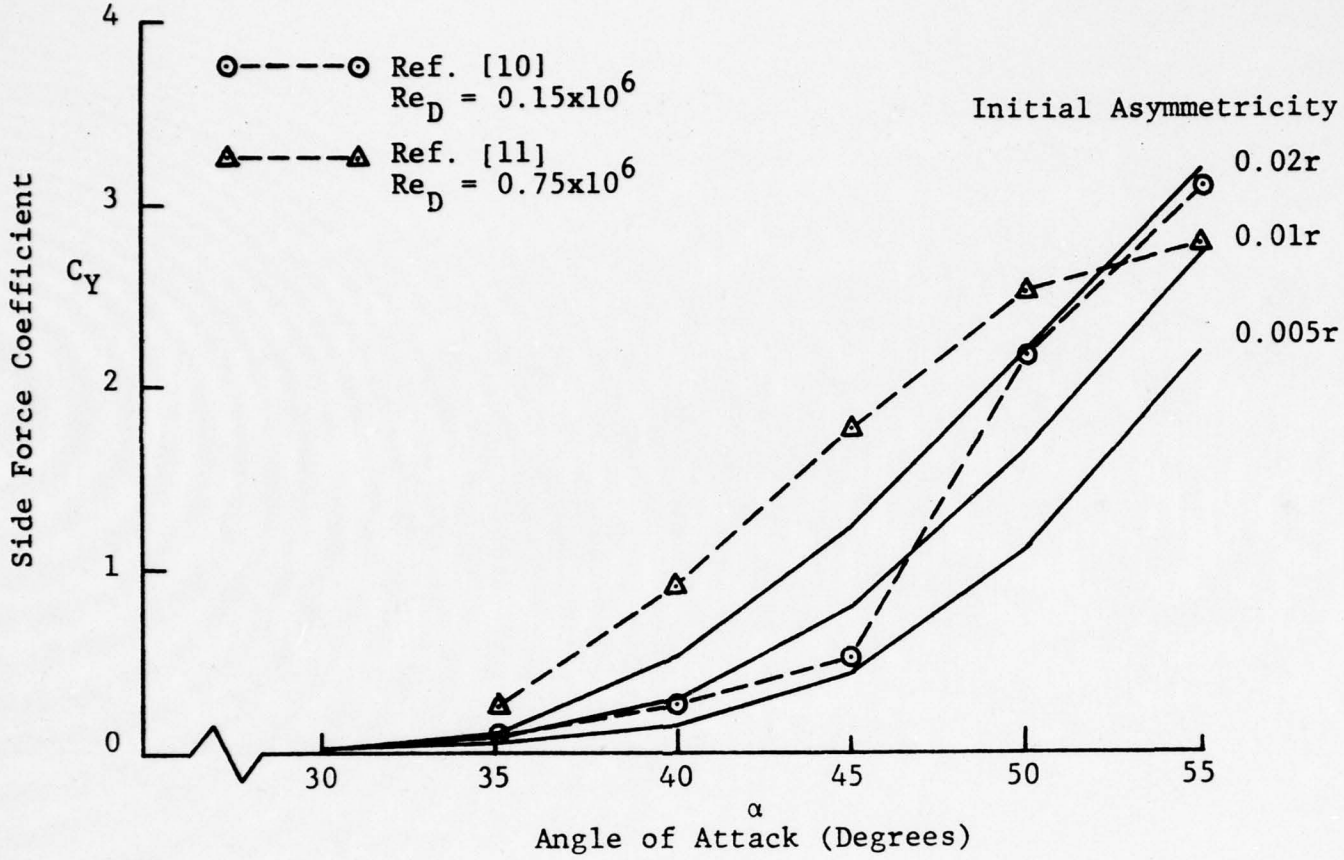

Figure 33. Side Force Coefficient vs. Angles of Attack for Ogive Forebody (Case 2).

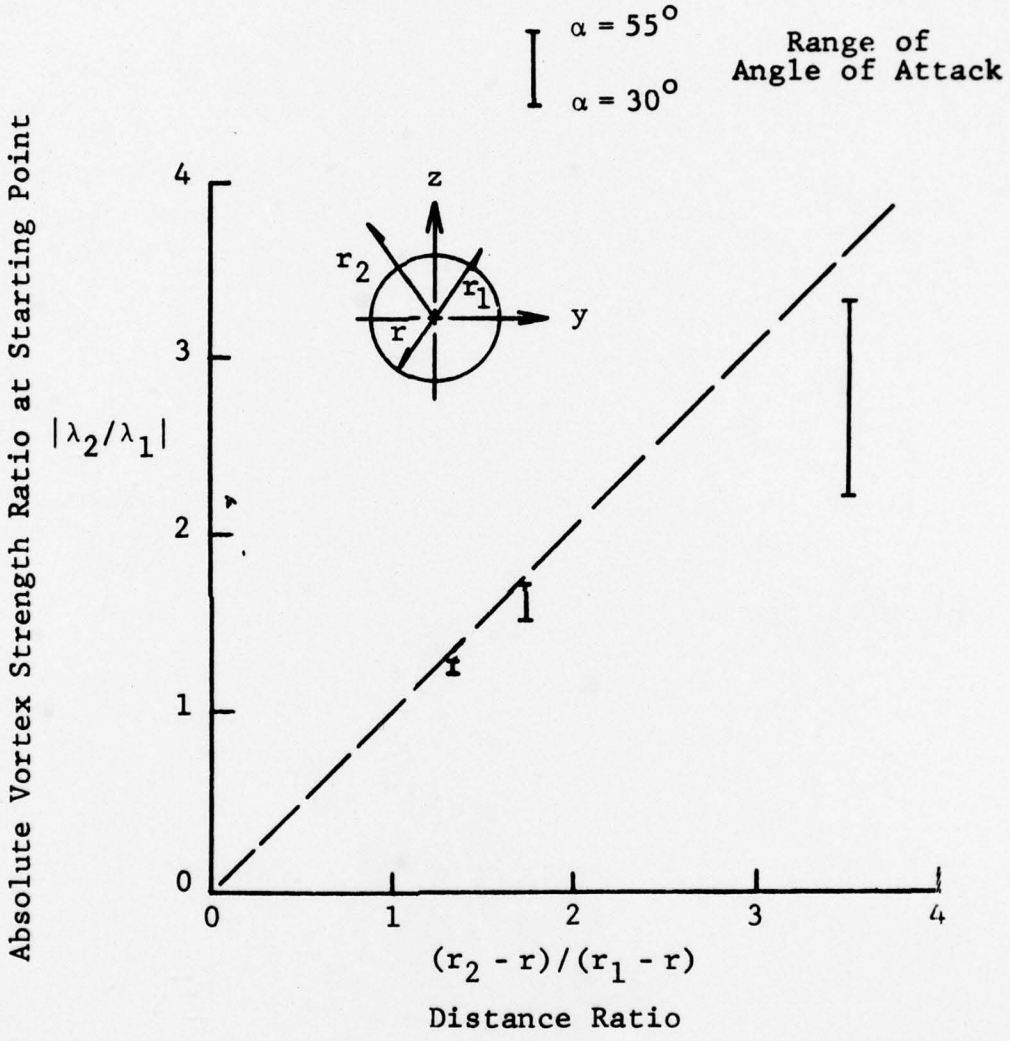

Figure 34. Absolute Vortex Strength Ratio at Starting Point vs. Distance Ratio.

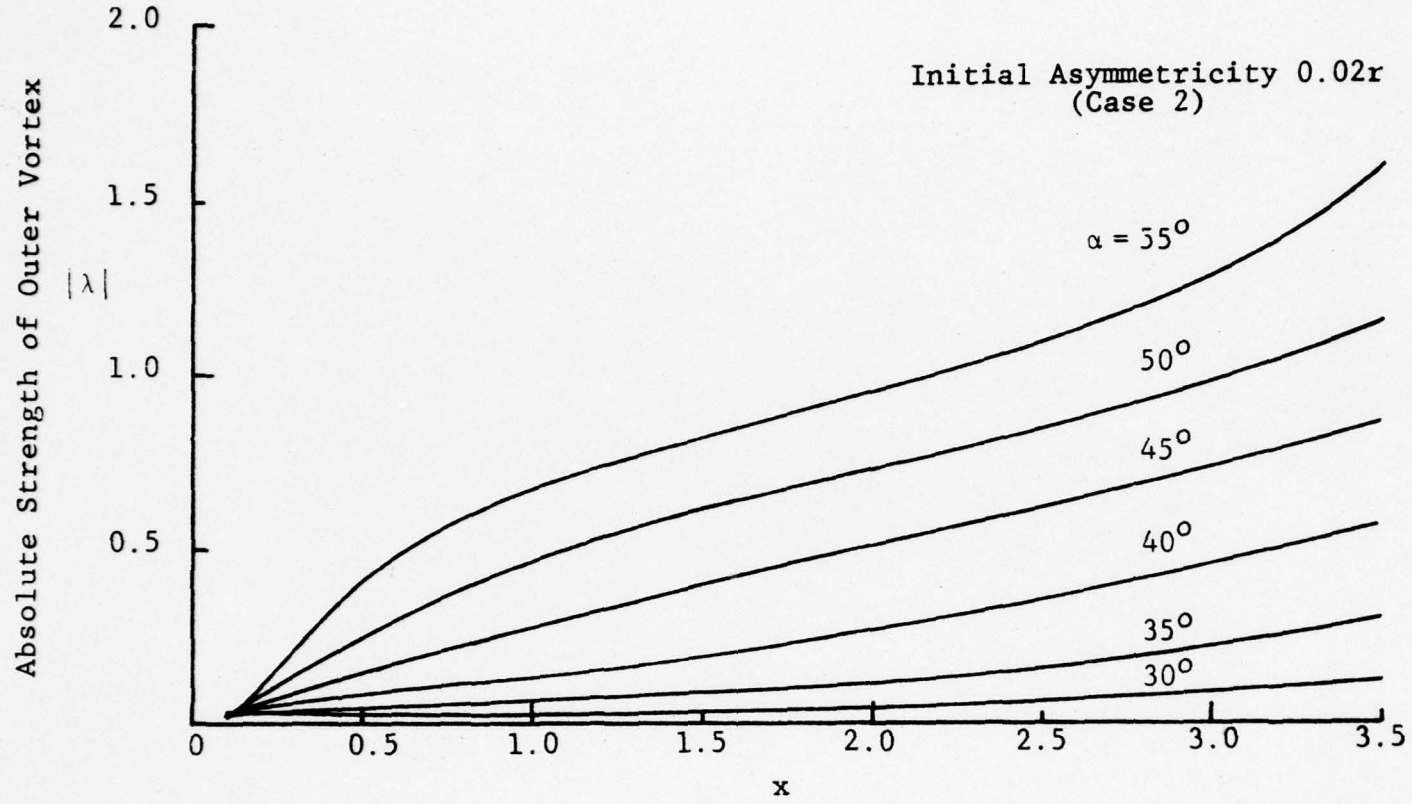

Figure 35. The Strength of Outer Vortex Along x-Axis for Ogive Forebody (Case 2).

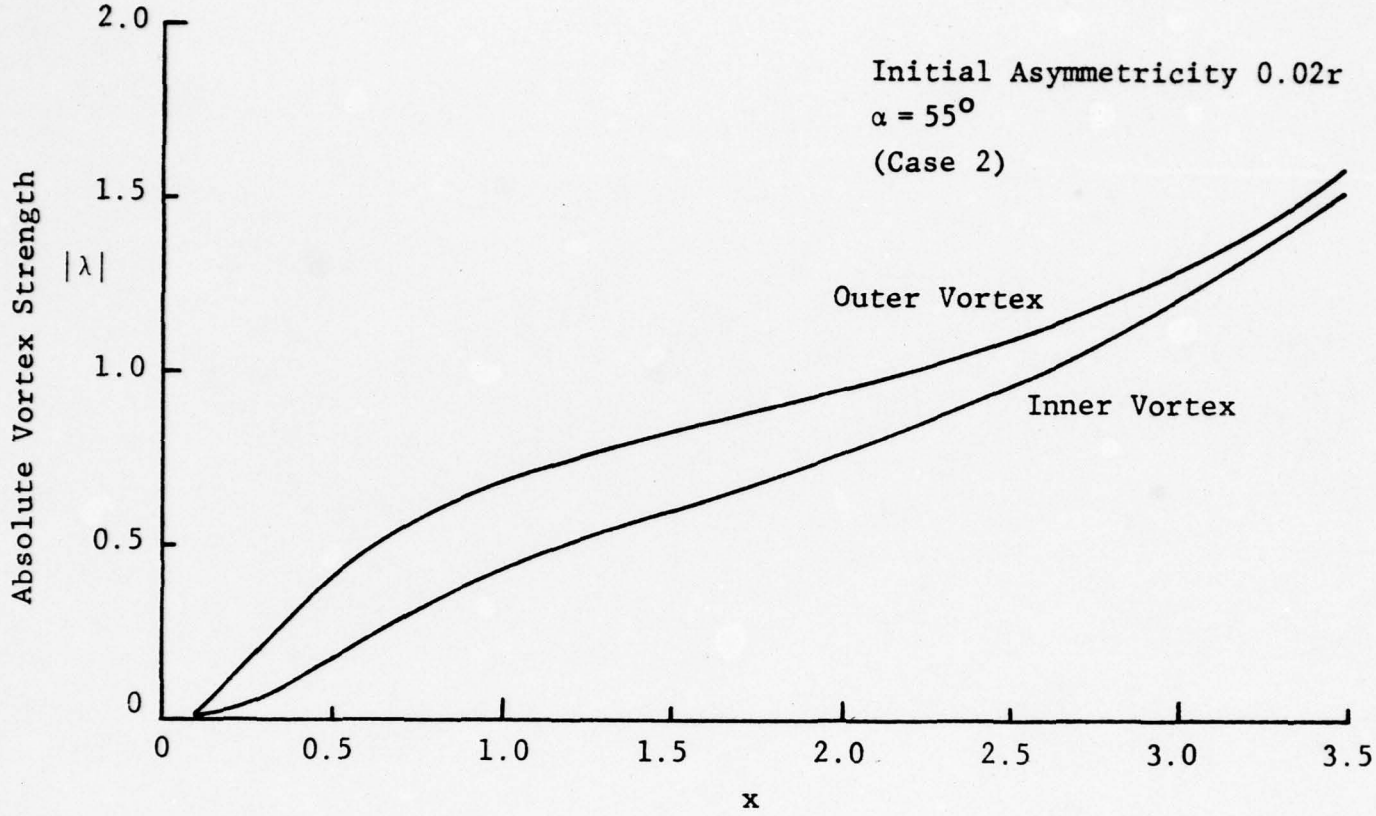

Figure 36. The Strength of Inner and Outer Vortex Along x-Axis for Ogive Forebody (Case 2).

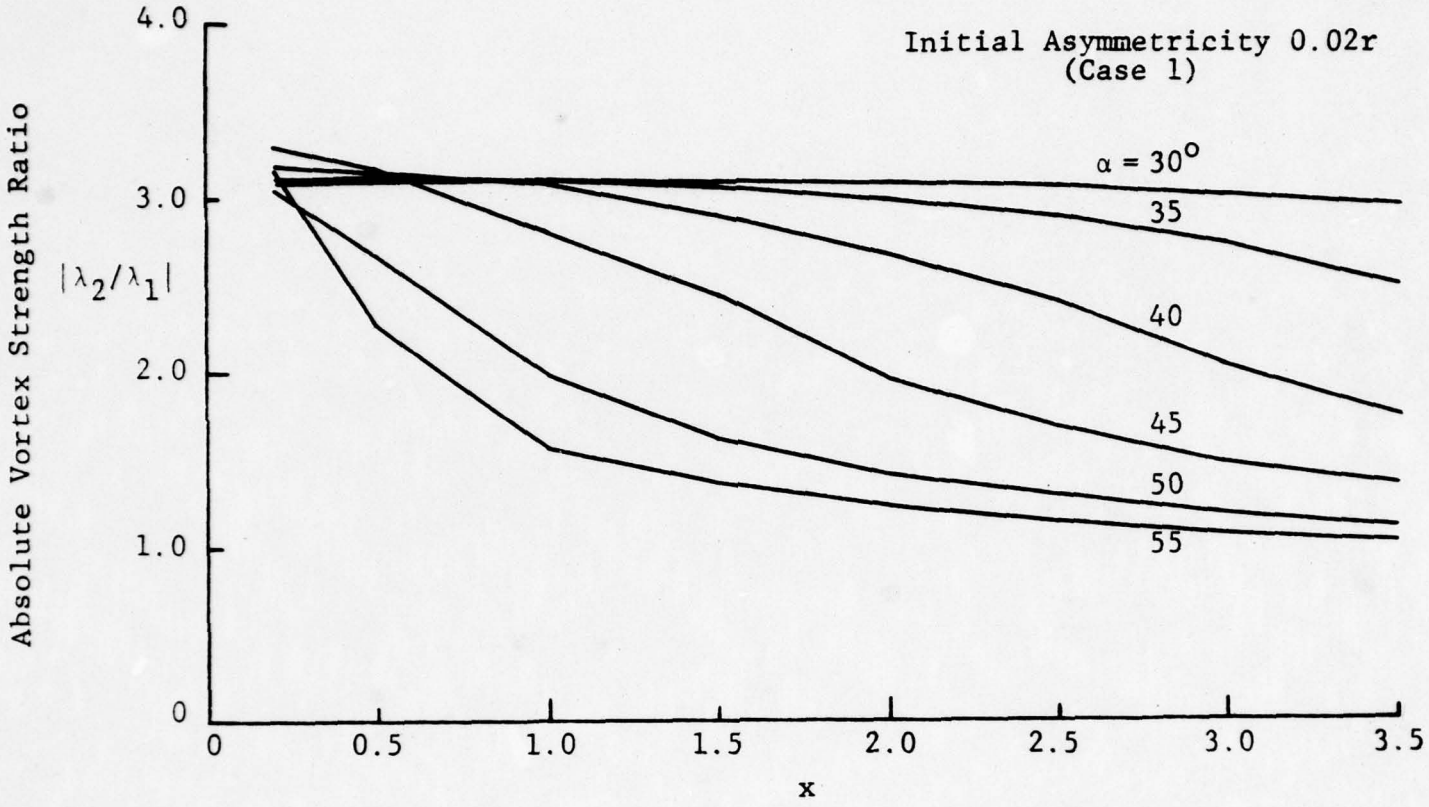

Figure 37. The Vortex Strength Ratio Along x-Axis (Case 1).

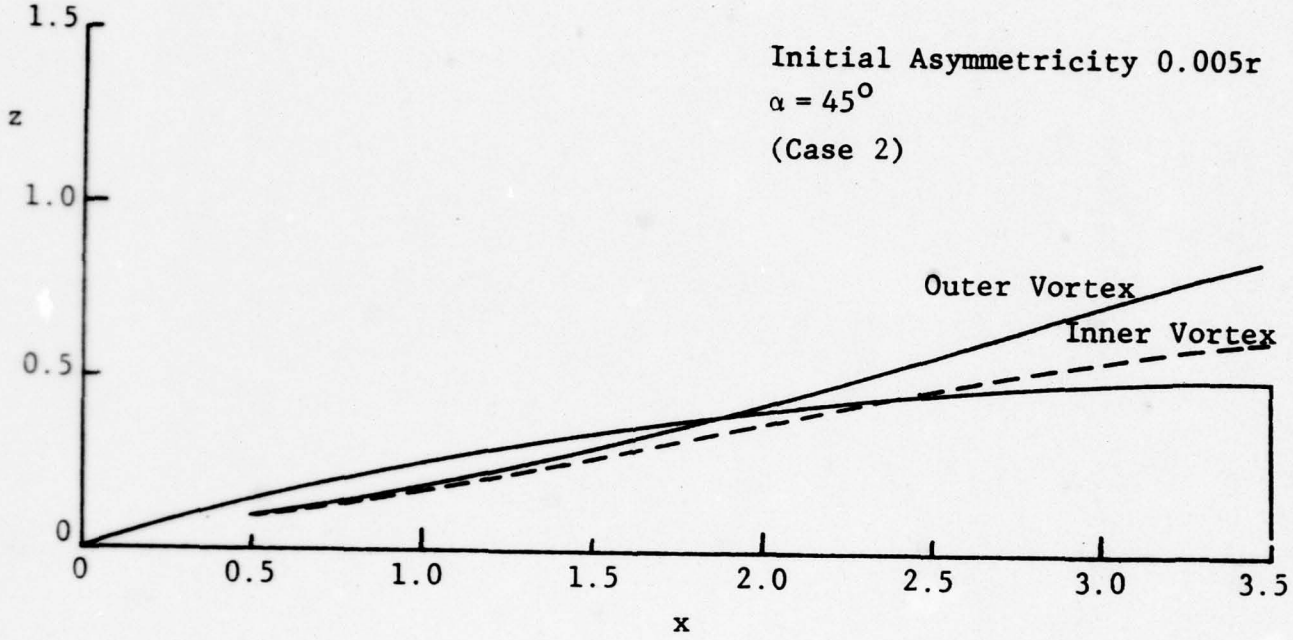

Figure 38. The Trace of the Inner and Outer Vortex Along x-Axis (Case 2).

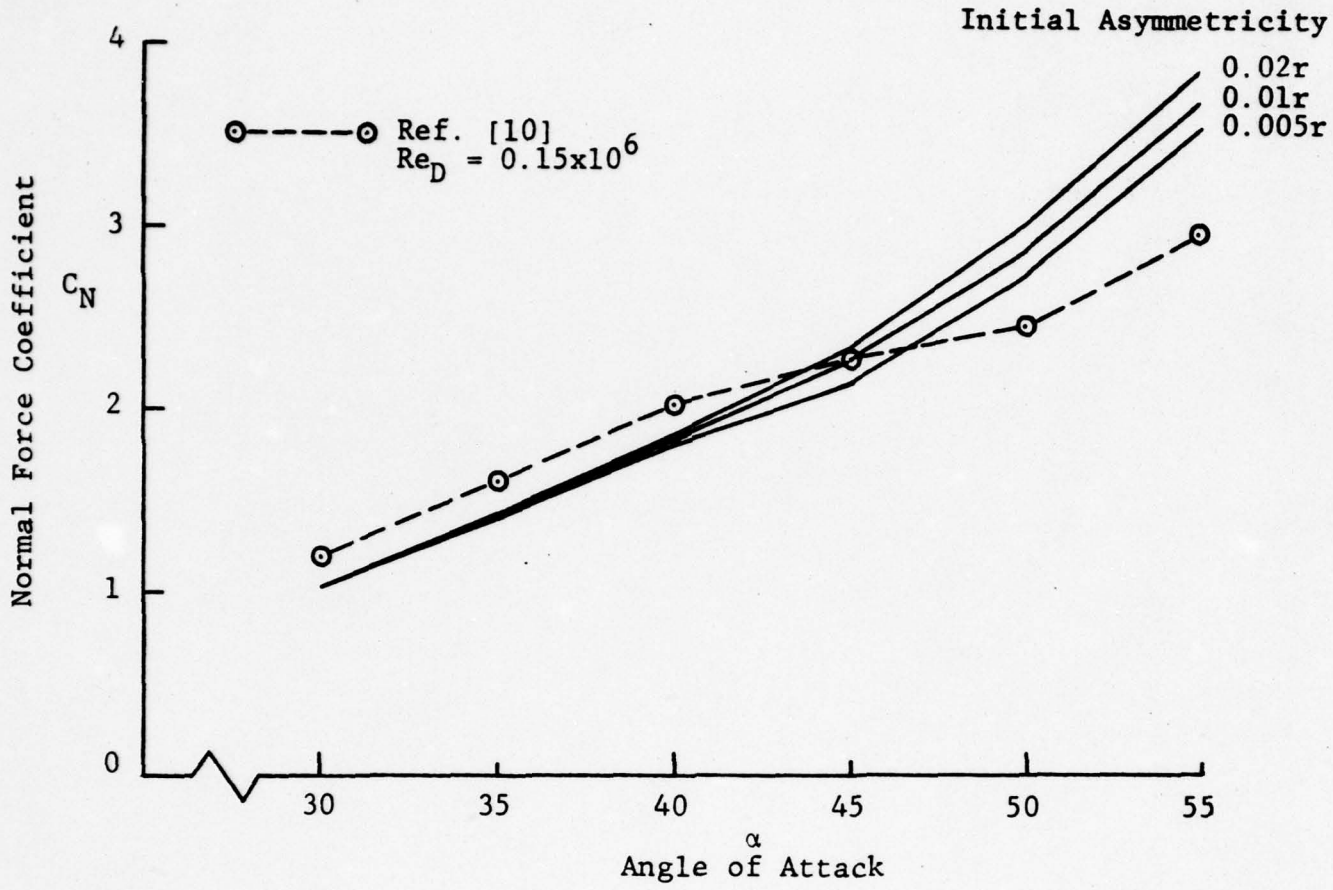

Figure 39. Normal Force Coefficient vs. Angles of Attack for Conical Forebody (Case 2).

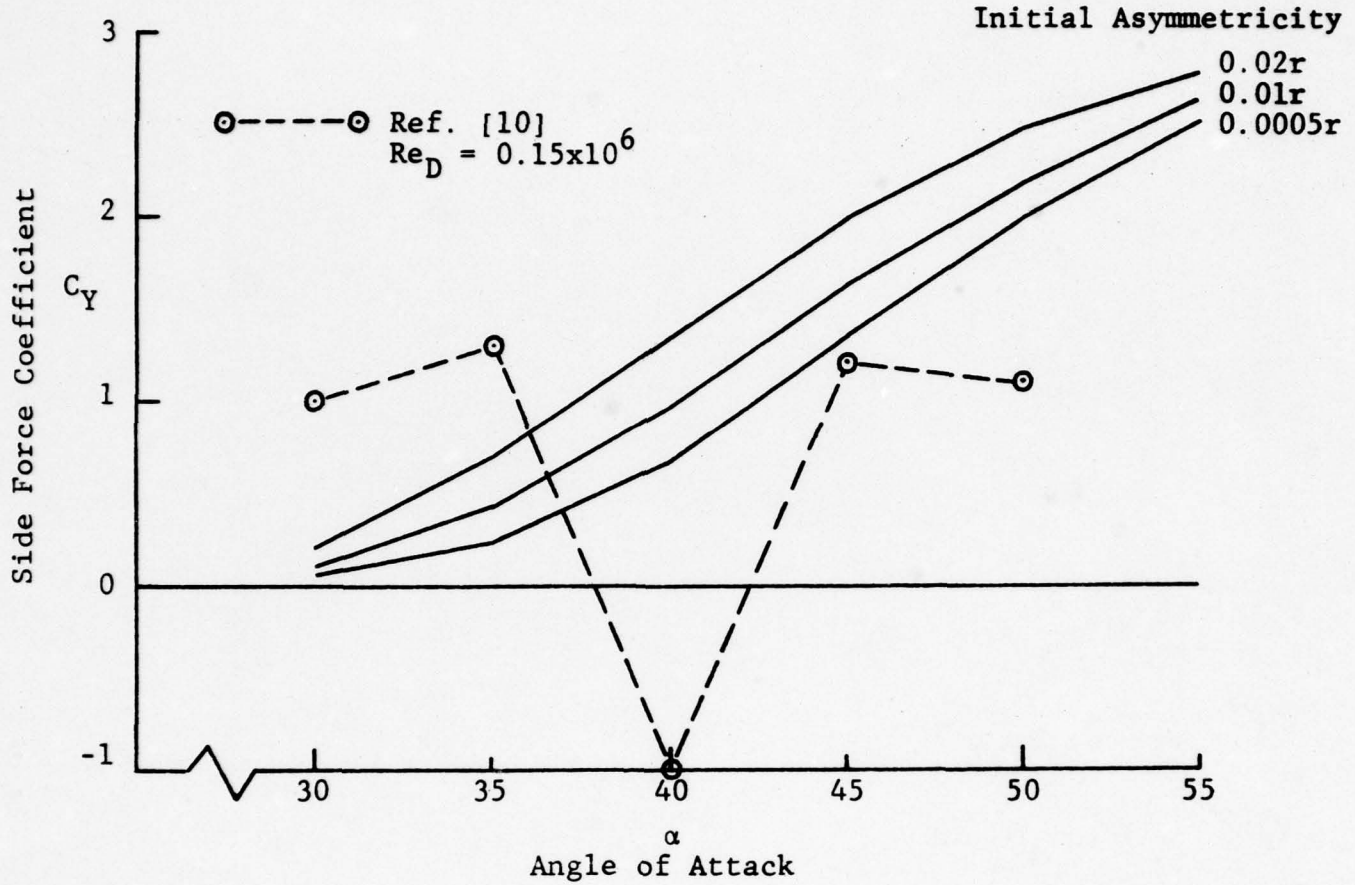

Figure 40. Side Force Coefficient vs. Angles of Attack for Conical Forebody (Case 2).

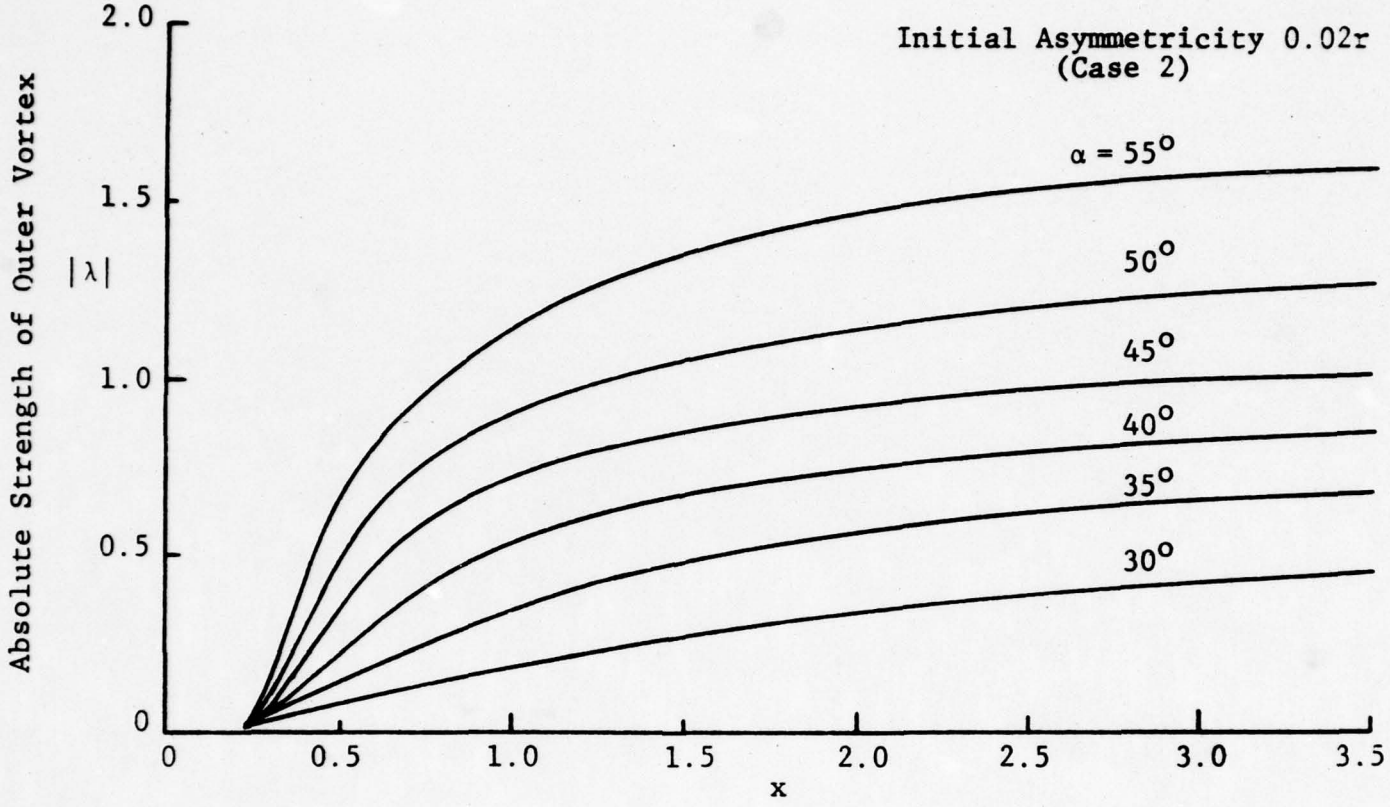

Figure 41. The Absolute Strength of Outer Vortex Along x-Axis (Case 2).

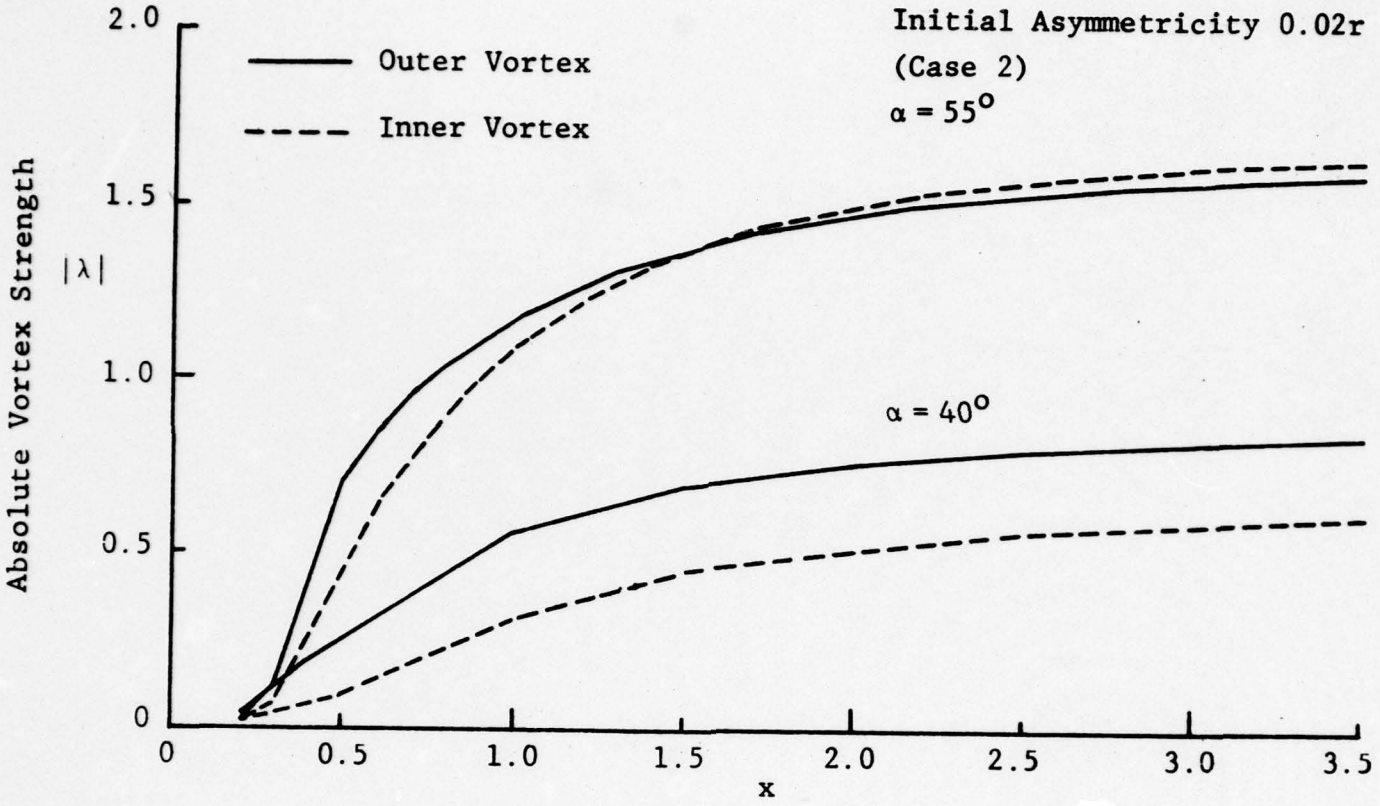

Figure 42. Absolute Strength of Inner and Outer Vortex at 40 and 55 Degrees in Angle of Attack (Case 2).

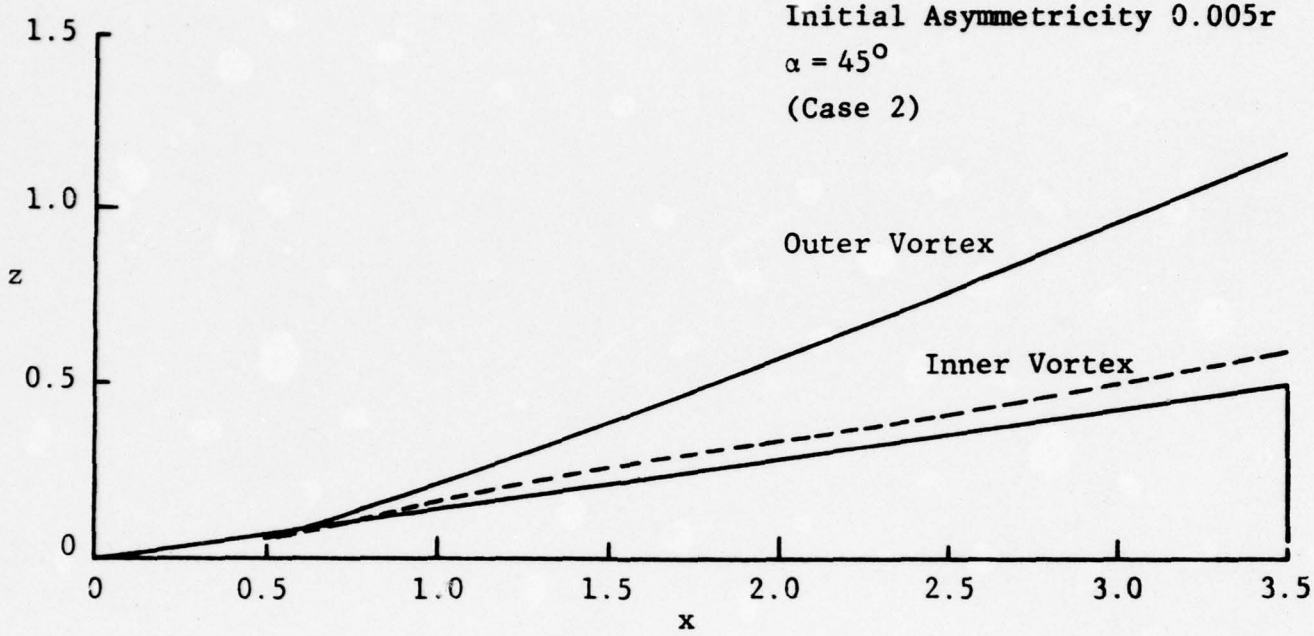

Figure 43. The Trace of Inner Vortex and Outer Vortex Along x-Axis (Case 2).

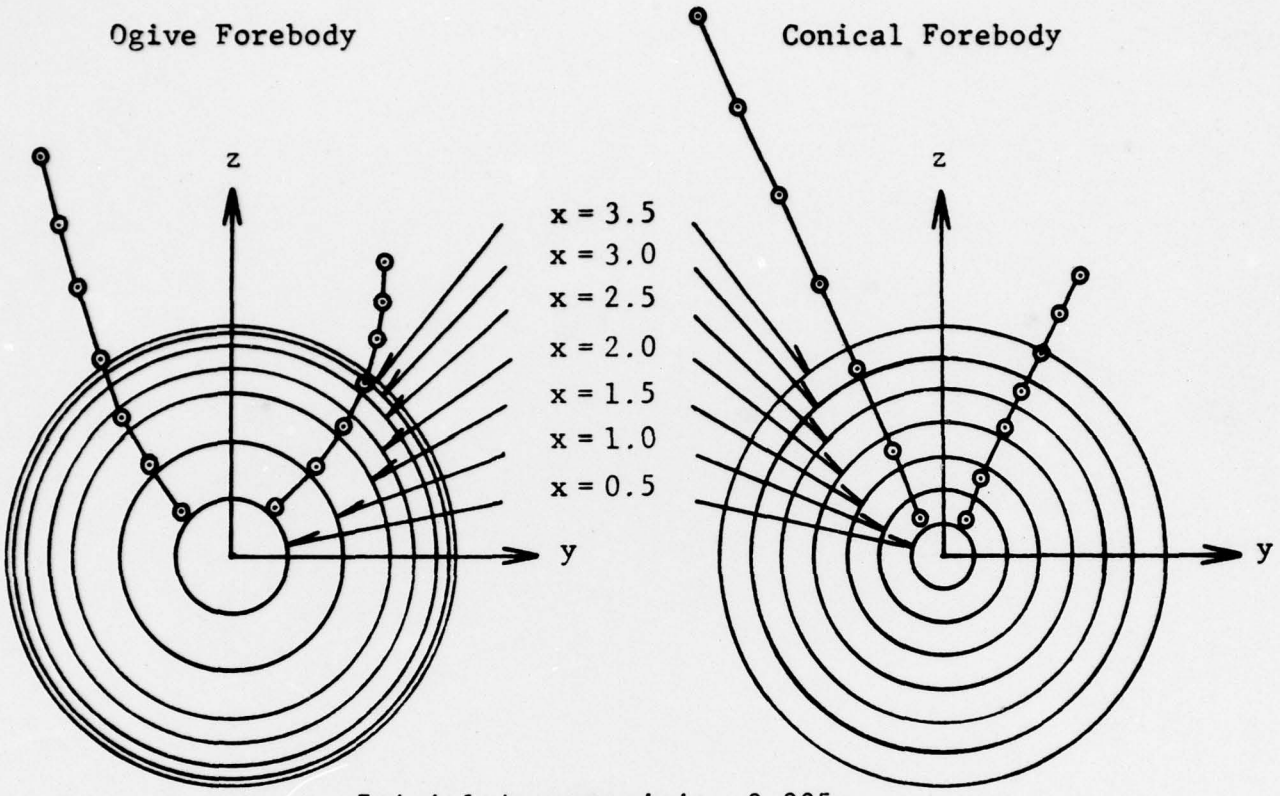

Figure 44. Comparison of the Vortex Traces Between Ogive and Conical Forebody (Case 2). (Viewed from front.)